J Neurophysiol 103: 1937–1953, 2010.
First published January 27, 2010; doi:10.1152/jn.00795.2009.

Simulating Microinjection Experiments in a Novel Model of the Rat Sleep-Wake Regulatory Network

Cecilia G. Diniz Behn[1] and Victoria Booth[1,2]
[1]*Departments of Mathematics and* [2]*Anesthesiology, University of Michigan, Ann Arbor, Michigan*

Submitted 25 August 2009; accepted in final form 22 January 2010

Diniz Behn CG, Booth V. Simulating microinjection experiments in a novel model of the rat sleep-wake regulatory network. *J Neurophysiol* 103: 1937–1953, 2010. First published January 27, 2010; doi:10.1152/jn.00795.2009. This study presents a novel mathematical modeling framework that is uniquely suited to investigating the structure and dynamics of the sleep-wake regulatory network in the brain stem and hypothalamus. It is based on a population firing rate model formalism that is modified to explicitly include concentration levels of neurotransmitters released to postsynaptic populations. Using this framework, interactions among primary brain stem and hypothalamic neuronal nuclei involved in rat sleep-wake regulation are modeled. The model network captures realistic rat polyphasic sleep-wake behavior consisting of wake, rapid eye movement (REM) sleep, and non-REM (NREM) sleep states. Network dynamics include a cyclic pattern of NREM sleep, REM sleep, and wake states that is disrupted by simulated variability of neurotransmitter release and external noise to the network. Explicit modeling of neurotransmitter concentrations allows for simulations of microinjections of neurotransmitter agonists and antagonists into a key wake-promoting population, the locus coeruleus (LC). Effects of these simulated microinjections on sleep-wake states are tracked and compared with experimental observations. Agonist/antagonist pairs, which are presumed to have opposing effects on LC activity, do not generally induce opposing effects on sleep-wake patterning because of multiple mechanisms for LC activation in the network. Also, different agents, which are presumed to have parallel effects on LC activity, do not induce parallel effects on sleep-wake patterning because of differences in the state dependence or independence of agonist and antagonist action. These simulation results highlight the utility of formal mathematical modeling for constraining conceptual models of the sleep-wake regulatory network.

INTRODUCTION

Studies of the brain stem and hypothalamic neuronal populations involved in the regulation of sleep and wake states suggest that changes in neurotransmitter levels play an important role in the initiation and maintenance of sleep-wake behavior (see Lydic and Baghdoyan 2005, 2008 for review). For example, wakefulness is characterized by the expression of high levels of noradrenaline by the locus coeruleus (LC), serotonin by the dorsal raphe (DR), and acetylcholine by pontine nuclei including the laterodorsal tegmentum (LDT) and the pendunculopontine tegmentum (PPT) through the ascending reticular activation pathway to thalamocortical regions. In contrast, sleep states are generally characterized by a reduction in the levels of all these neurotransmitters in higher brain regions with the exception of acetylcholine which returns to waking levels during rapid eye movement (REM) sleep.

Address for reprint requests and other correspondence: V. Booth, Dept. of Mathematics, Univ. of Michigan, 2074 East Hall, 530 Church St., Ann Arbor, MI 48109 (E-mail: vbooth@umich.edu).

The regulation of the expression of these neurotransmitters results from modulation of activity in the associated neuronal nuclei by network interactions. Although the LC and DR are accepted components of the sleep-wake network, recent anatomical and physiological studies have identified new brain stem and hypothalamic populations that may be involved in the network and have proposed different versions of network architecture (Saper et al. 2005). Network components involved in the regulation of REM sleep have been of particular interest. The classical conceptual model has been one of cholinergic regulation of REM sleep, proposed by McCarley and Hobson (1975), wherein reciprocal interactions between monoaminergic REM-off populations and cholinergic REM-on pontine populations govern transitions between non-REM (NREM) and REM sleep. More recent studies have implicated a role for GABA in the control of REM sleep (Brown et al. 2008; Datta and Maclean 2007; Lu et al. 2004; Luppi et al. 2006; Mallick et al. 2001; Sapin et al. 2009). However, the exact architecture of the regulatory network has not been completely determined.

We propose a mathematical modeling framework that is uniquely suited for investigating the structure and dynamics of the sleep-wake regulatory network. This framework is based on a novel population firing rate model formalism in which we modify the traditional firing rate model formalism to explicitly include neurotransmitter concentration variables reflecting the release of transmitter to postsynaptic targets. The dynamics of neurotransmitter concentrations follow saturating expression profiles consistent with experimental observations. Coupling between populations occurs as a result of transmitter concentration levels in postsynaptic populations. In this formalism, time scales characteristic of specific neurotransmitter expression in postsynaptic targets or of postsynaptic receptor activation can be explicitly distinguished. More importantly, experimental studies have manipulated the neurotransmitter environments in specific nuclei through targeted microinjection of transmitter agonists and antagonists to probe the regulatory network. Our modeling formalism allows direct simulation of this type of experimental protocol.

The specific network structure of brain stem and hypothalamic nuclei that we consider is based on known neural pathways and neurotransmitter effects. It includes the mutual inhibitory interaction between wake-promoting nuclei in the brain stem and sleep-promoting nuclei in the hypothalamus that forms the basis of the conceptual flip-flop model for sleep generation (Saper et al. 2001). It also contains reciprocal interactions between pontine REM-promoting nuclei and wake-promoting nuclei, whose activity ceases during REM sleep, similar to the reciprocal interaction model for REM regulation (Massaquoi and McCarley 1992; McCarley and Hobson 1975). The network structure is similar to that used in other mathematical models of the sleep-wake regu-

latory network (Diniz Behn et al. 2007; Phillips and Robinson 2007; Tamakawa et al. 2006) and focuses on primary mechanisms. However, this structure is not comprehensive, and some neurotransmitters and neuropeptides involved in modulating sleep-wake behavior, such as orexin/hypocretin and dopamine (Dzirasa et al. 2006; Nakamura et al. 2000; Peyron et al. 1998; Rye and Jankovic 2002; Thannickal et al. 2000), are not included. We analyze how this network structure can account for typical rat sleep-wake patterning and describe how specific components of the structure support interaction dynamics consistent with experimental observations.

To probe network structure and dynamics, we simulate microinjections of neurotransmitter agonists and antagonists into one neuronal nucleus, namely the LC, and analyze effects on sleep-wake patterning. We particularly study whether agonist/antagonist pairs, which are presumed to have opposing effects on LC activity, generally induce opposing effects on sleep-wake patterning in the network. Experimental results suggest that opposing effects are obtained for some sleep-wake states, such as waking or REM sleep (Mallick et al. 2001), but trends are not as clear for all sleep states, particularly because many studies report only on percent time spent in specific states rather than on details of sleep microarchitecture. A focus of our simulations of these experiments is to track effects on all states and analyze indirect effects of manipulations of just one population that are propagated through the network to impact activation of other nuclei and resultant patterning of all sleep-wake states. We also analyze if different agents, which are presumed to have parallel effects on activity of a given nucleus, induce parallel effects on network dynamics and sleep-wake patterning. For example, GABA agonists and cholinergic antagonists have both been shown to attenuate LC activity (Ennis and Shipley 1992; Osmanovic and Shefner 1990); however, experimental studies have suggested that each has a different effect on sleep states (Mallick et al. 2001). We analyze our simulation results to determine specific actions of each agent and elucidate the differences in effects of parallel agents.

METHODS

We first generally describe the formalism of our novel firing rate model and how microinjection of neurotransmitter agonists and antagonists can be simulated. We then describe the model of the sleep-wake regulatory network constructed with this formalism. The complete equations and parameter values for the sleep-wake network model are given in the APPENDIX.

Firing rate model formalism

We propose a novel firing rate model formalism for the interaction of neuronal populations that explicitly includes neurotransmitter concentrations released by presynaptic populations. The dynamics of neurotransmitter concentrations drive the response of postsynaptic populations (Fig. 1*A*).

Standard firing rate models provide a formalism for determining the relationships between activity of presynaptic populations, total synaptic input to a postsynaptic population, and the resulting postsynaptic firing rate (Deco et al. 2008; Wilson and Cowan 1972; see reviews in Dayan and Abbott 2001; Deco et al. 2008; Ermentrout 1998). Typically, the total synaptic input is determined by a weighted sum of the presynaptic firing rates, and the firing rate of the postsynaptic population evolves to a nonlinear function of the total synaptic input with some characteristic time constant. In our model, we retain this basic formalism but replace total synaptic input with a weighted sum of neurotransmitter concentrations released by presynaptic populations, $C_i(t)$, where the subscript i allows for multiple neurotransmitters. In this way, firing rate in a postsynaptic population X, $F_X(t)$, is modeled by the standard equation of the following form

$$F'_X = \frac{F_{X\infty}\left(\sum_i g_{i,X} C_i\right) - F_X}{\tau_X} \quad (1)$$

where the steady-state firing rate $F_{x\infty}(\cdot)$ is a saturating function, the $g_{i,X}$ are constant weights, and τ_X is the time constant associated with the response of the postsynaptic population. For the steady-state firing rate function, we use the standard sigmoidal function

$$F_{X\infty}(c) = X_{max}\,(0.5\{1 + \tanh[(c - \beta_X)/\alpha_X)]\}) \quad (2)$$

characterized by parameters X_{max}, α_X, and β_X (Fig. 1*B*). This functional form ensures that sufficient release of inhibitory neurotransmitters silences the population and excessive release of excitatory neurotransmitters causes firing to saturate at a maximal rate, X_{max}. Intrinsic population properties such as excitability of individual neurons and local connectivity can be used to determine the parameters governing the slope of the sigmoid (α_X) and the activation threshold (β_X).

Neurotransmitter concentration, $C_i(t)$, depends on the firing rate of the presynaptic population, generically referred to as $F_Y(t)$. In our formalism, $C_i(t)$ evolves to a nonlinear function of $F_Y(t)$ as described by the following equation

$$C'_i = \frac{C_{i\infty}(F_Y) - C_i}{\tau_i} \quad (3)$$

where steady-state neurotransmitter release, $C_{i\infty}(\cdot)$, is a saturating function and τ_i is the associated time constant. Because different microdialysis techniques lead to differences in absolute reported neurotransmitter concentrations, we normalize each neurotransmitter concentration between 0 and 1. The functional form of $C_{i\infty}(\cdot)$, $C_{i\infty}(f) = \tanh(f/\gamma_i)$, prescribes the relationship between presynaptic firing rate and neurotransmitter release, and the shape of this function was chosen to be consistent with experimental data (Aston-Jones and Bloom 1981; Lydic and Baghdoyan 1993) (Fig. 1*C*). In particular, neurotransmitter concentration increases monotonically with presynaptic firing rate and approaches a saturating level (normalized to 1) at maximum firing rate. The time scale described by τ_i reflects the time dynamics associated with neurotransmitter release at the level of the population rather than at an individual synapse. The temporal resolution of current microdialysis techniques does not allow direct measurement of τ_i. However, recent results using voltammetric techniques have shown that the rate constants for release and clearance of evoked dopamine are on the order of seconds (Garris and Wightman 1994), and we chose values for τ_i to be consistent with this result.

In a network model, all coupling between populations is mediated through neurotransmitter concentrations: $C_{i\infty}(\cdot)$ describes how firing activity in the presynaptic population results in production of neurotransmitter, and $F_{X\infty}(\cdot)$ determines how neurotransmitter levels affect activity in the postsynaptic population. By explicitly modeling the dynamics of each neurotransmitter, the formalism allows for distinct time scales associated with the release of each neurotransmitter or with specific postsynaptic receptor dynamics. This contrasts with many firing rate model formalisms in which the dynamics of inputs from all presynaptic sources are described by a single time constant (Dayan and Abbott 2001; Deco et al. 2008; Phillips and Robinson 2007, 2008; Wilson and Cowan 1972). A more detailed comparison of our formalism with other firing rate models is provided in the DISCUSSION.

Neurotransmitter release is correlated with, but not determined by, the firing rate of the presynaptic population, and variability of release grows with concentration level (Aston-Jones and Bloom 1981). This

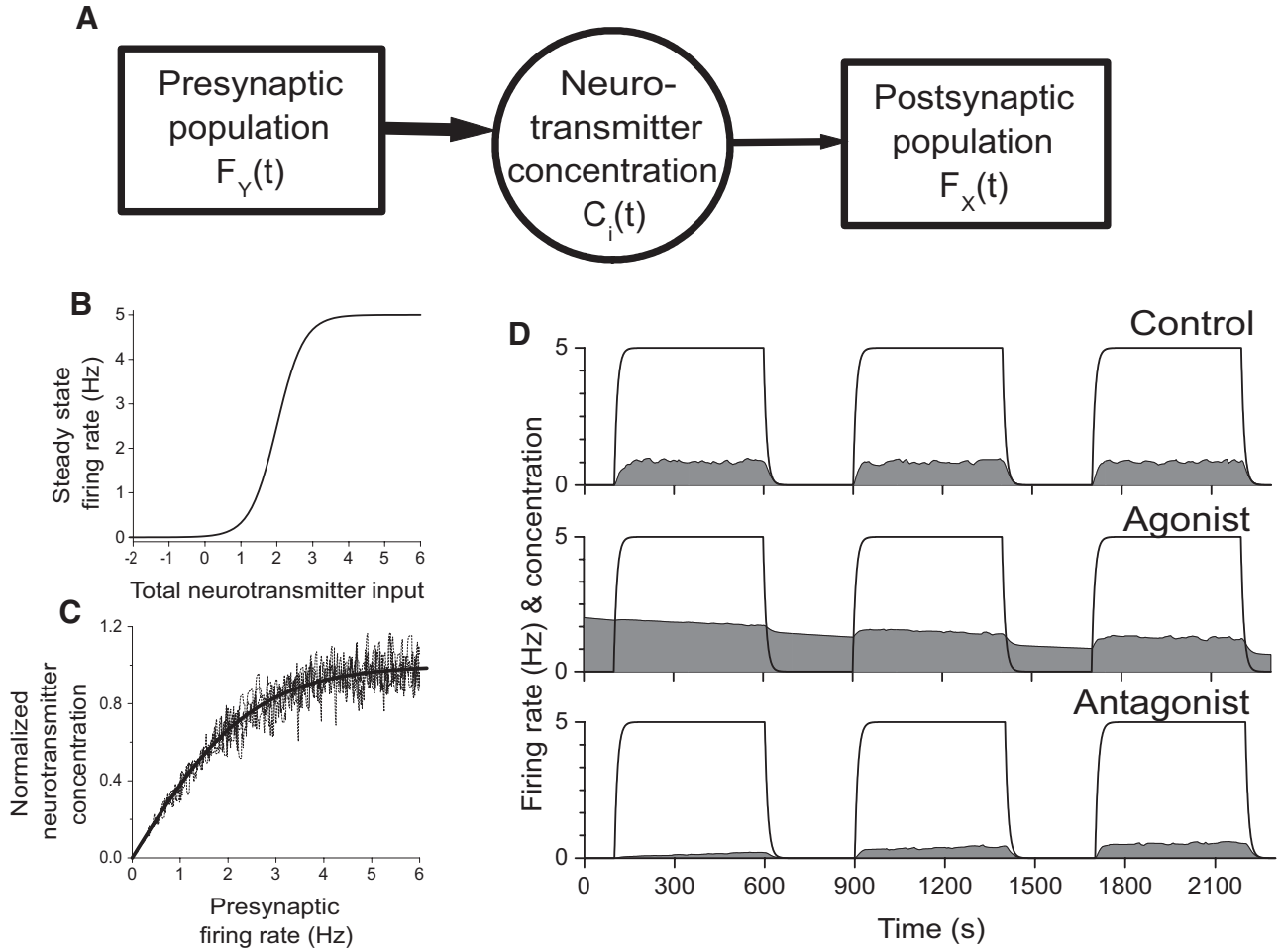

FIG. 1. The key elements of the proposed firing rate model formalism. *A*: activity in a presynaptic population, $F_Y(t)$, generates neurotransmitter release, $C_i(t)$, which affects activity in the postsynaptic population, $F_X(t)$. Therefore the effect of the presynaptic population on the postsynaptic population is explicitly mediated through the presynaptic population's associated neurotransmitter. *B*: steady-state firing rate profile of postsynaptic population $F_{X\infty}(\cdot)$ is a saturating sigmoidal function of weighted input of neurotransmitters released by presynaptic populations (representative example shown). *C*: steady-state neurotransmitter release profile $C_{i\infty}(\cdot)$ (thick line) is a function of firing rate in the presynaptic population, but a multiplicative noisy scaling factor creates a family of steady-state neurotransmitter release profiles (thin lines) reflecting the physiological variability in neurotransmitter release (representative example shown). *D*: activity in the presynaptic population (curve) drives neurotransmitter concentration in a postsynaptic population (shaded region, representative examples shown). Control: maximum activation of the presynaptic population results in maximum transmitter release in the postsynaptic population. Agonist: after microinjection of neurotransmitter agonist into the postsynaptic population, changes in neurotransmitter concentration reflect both the slow decay of the microinjected agonist from an elevated initial level and a concentration-dependent attenuation of endogenous neurotransmitter release. Antagonist: after microinjection of neurotransmitter antagonist into the postsynaptic population, transmitter concentration reveals scaling of the effects of endogenous released neurotransmitter; in the absence of endogenous neurotransmitter, the antagonist does not have an effect.

represents a key source for physiological noise in our formalism. To incorporate this variability of neurotransmitter release into the model, the steady-state neurotransmitter release function $C_{i\infty}(\cdot)$, was multiplicatively scaled by a noise factor, $\sigma_i(t)$, whose amplitude randomly varied (with normal distribution and unit mean) according to a Poisson process. This mechanism introduced a time-varying element into steady-state neurotransmitter release and resulted in variable target neurotransmitter concentrations for fixed presynaptic firing rates (Fig. 1*C*). Furthermore, the use of a scaling factor resulted in concentration-dependent variability consistent with experimental data (Aston-Jones and Bloom 1981). In addition, variability in the firing thresholds of individual neurons in postsynaptic populations is accounted for in the sigmoidal shape of the steady-state firing rate function, $F_{X\infty}(\cdot)$, as in other firing rate models.

Simulating microinjection experiments

To simulate microinjection of neurotransmitter agonists and antagonists in this modeling framework, we introduced a variable for concentration levels of each agonist and antagonist in the targeted population. The agonist and antagonist variables were denoted by $P_i(t)$ and $Q_i(t)$, respectively, where i indicates the affected transmitter. The dynamics of the agonist and antagonist variables are described by a positive initial value, simulating the bolus injection, followed by a slow decay representing diffusion and reuptake. The slow decay is governed by a time constant, τ_{Pi} or τ_{Qi}, that is chosen to reflect the time scale of the observed effects of the agonist or antagonist

$$\frac{dP_i}{dt} = -\frac{P_i}{\tau_{Pi}} \quad \text{and} \quad \frac{dQ_i}{dt} = -\frac{Q_i}{\tau_{Qi}} \tag{4}$$

For the microinjection experiments we simulate, these effects last for ~4 h (Mallick et al. 2001).

We model the net effect of the endogenously released neurotransmitter and the injected neurotransmitter agonist or antagonist by appropriately scaling or augmenting endogenous neurotransmitter in the targeted population. High concentrations of injected neurotransmitter or neurotransmitter agonist often affect the release of endoge-

nous neurotransmitter (Kalsner 1990; Starke et al. 1989). To reflect this interaction in agonist microinjection simulations, we replace the variable for endogeneous neurotransmitter concentration as released by the presynaptic population, $C_i(t)$, in the targeted population X with the following expression

$$C_{i(X)}(t) = m_i(t)C_i(t) + P_i(t) \quad (5)$$

The scaling factor $m_i(t)$ reflects the effect of the agonist on transmitter release. It is set to 1 if P_i levels are low (less than a specified minimum value) but, for higher P_i levels, it increases from 0 to 1 as P_i decreases from a maximum initial value (Fig. 1*D*, *middle*).

To capture the decrease in the effects of endogenous neurotransmitter caused by microinjection of an antagonist, we replace the variable for endogeneous neurotransmitter concentration, $C_i(t)$, in the target population X with a value scaled by the level of antagonist

$$C_{i(X)}(t) = [1 - Q_i(t)]C_i(t) \quad (6)$$

As Q_i decays to 0, transmitter concentration in the target population, $C_{i(X)}$, regains the full level of transmitter released by the presynaptic population, $C_i(t)$ (Fig. 1*D*, *bottom*).

Applying the neurotransmitter model formalism to a sleep-wake regulatory network

Using the firing rate model formalism described above, we constructed a model of the rodent sleep-wake regulatory network (Fig. 2). This formalism is well suited to model neural regulation of sleep-wake behavior because specific patterns of spike timing in the constituent neuronal populations seem to be less important in supporting each behavioral state compared with the overall profiles of population activity and resultant neurotransmitter release. The structure of the network model was based on experimental characterization of the relevant anatomy and physiology (see Saper et al. 2005 for review). The network included wake-promoting, sleep-promoting, and REM sleep-promoting neuronal populations and their associated neurotransmitters (Table 1).

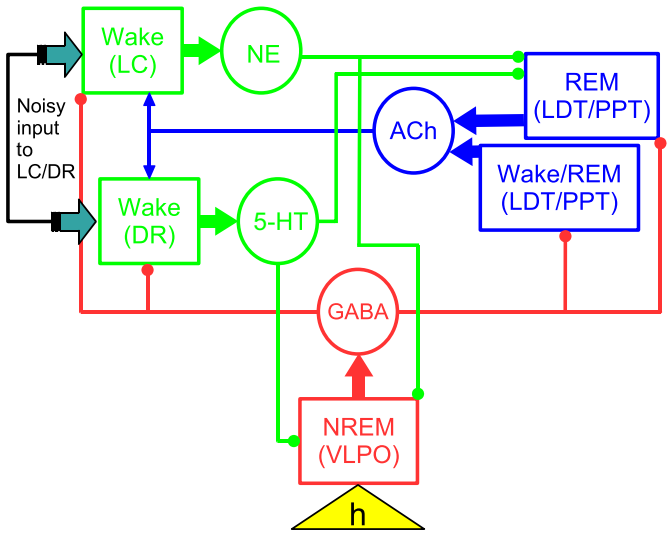

FIG. 2. Schematic of the model sleep-wake regulatory network (summarized in Table 1) shows interactions between wake-, non–rapid eye movement (NREM)-, and REM-promoting neuronal populations (rectangles) mediated through their associated neurotransmitters (circles). The homeostatic sleep drive *h* (yellow triangle) represents adenosinergic modulation of baseline activity in the sleep-promoting ventrolateral preoptic nucleus (VLPO). In addition, synaptic input from thalamocortical networks to locus coeruleus (LC) and dorsal raphe (DR) (teal arrows) are modeled with random excitatory inputs.

TABLE 1. *Summary of the wake-, sleep-, and REM-sleep promoting neuronal populations and associated neurotransmitters included in the model network*

	Population	Neurotransmitter
Wake-promoting	Dorsal raphe (DR)	Serotonin (5-HT)
	Locus coeruleus (LC)	Noradrenaline (NE)
	Wake/REM active subpopulations (WR) of laterodorsal tegmental nucleus and pedunculopontine tegmental nucleus (LDT/PPT)	Acetylcholine (ACh)
Sleep-promoting	Ventrolateral preoptic area (VLPO)	GABA
REM-promoting	REM active subpopulation (R) of LDT/PPT	Acetylcholine (ACh)

Firing rates of each population, $F_X(t)$ (in Hz, $X = LC, DR, VLPO, R,$ or WR) are governed by equations of the form given in *Eq. 1* and the concentrations of neurotransmitter released by each population, $C_i(t)$ are described by equations of the form given in *Eq. 3* [$i = N$ (NE) for $Y = LC$; $i = S$ (5-HT) for $Y = DR$; i = G (GABA) for $Y = VLPO$; $i = A(R)$ (ACh) for $Y = R$; and $i = A(WR)$ (ACh) for $Y = WR$]. When possible, the parameter values in the model were based on experimental data (see APPENDIX for details).

The neurotransmitter-mediated coupling between populations included in the model network is based on established anatomy and physiology. Briefly, the monoaminergic wake-promoting populations, LC and DR, inhibit both the sleep-promoting VLPO and the REM-active subpopulation of the LDT/PPT, but not the wake/REM active LDT/PPT subpopulation (Thakkar et al. 1998). On the other hand, the sleep-promoting VLPO inhibits all wake-promoting and REM-promoting populations. The cholinergic REM- and wake/REM-active populations excite the LC and DR. These interactions are reflected in the terms included in the argument, $\sum_i g_{i,X} C_i$, of the steady-state firing rate functions, $F_{X\infty}(\cdot)$, for each population.

Within this network structure, specific subcomponents reflect conceptual models of the interaction of these populations that are current in the literature. Specifically, mutual inhibition between the monoaminergic wake-promoting populations (LC and DR) and the GABAergic sleep-promoting population (VLPO) provides the basis for the conceptual sleep-wake flip-flop switch (Saper et al. 2001) that is thought to be the generative mechanism for production of and transitions between NREM sleep and wake. Additionally, reciprocal connectivity between monoaminergic wake-promoting populations (LC and DR) and cholinergic REM-promoting populations (LDT/PPT) reflects the reciprocal interaction hypothesis of NREM-REM cycling (Massaquoi and McCarley 1992; McCarley and Hobson 1975). The LC, DR, and VLPO are modeled as self-inhibitory while self-excitatory projections are included in the cholinergic REM- and wake-promoting subpopulations of the LDT/PPT. This self-excitation reflects the glutamatergic positive feedback projection to the LDT/PPT via the pontine reticular formation (reviewed in Datta and Maclean 2007). In addition, random excitatory inputs to the wake-promoting populations (LC and DR) were included to simulate activity of top-down excitatory projections from thalamocortical circuits (Arnsten and Goldman-Rakic 1984; Jodo et al. 1998).

Homeostatic sleep drive h

The concept of a homeostatic sleep drive was formalized with the designation of "Process S" in the two process model of sleep regulation (Borbely 1982; Borbely and Achermann 1999). Process S describes a drive to sleep that increases during time awake and decreases during sleep. Although the biological substrate of homeostatic sleep drive probably involves multiple mechanisms, the neuromodulator adenosine is one important element (reviewed in Basheer et al. 2004;

Huang et al. 2007). Briefly, extracellular adenosine concentrations in the basal forebrain and cortex increase with time in wakefulness (Porkka-Heiskanen et al. 2000), microinjection of adenosine into these areas promotes sleep (Basheer et al. 1999; Van Dort et al. 2009), and microinjection of adenosine A1 receptor antagonist increases wakefulness (Thakkar et al. 2003; Van Dort et al. 2009). The somnogenic effect of adenosine may arise from the action of adenosine at several sites in the sleep-wake regulatory network: adenosine inhibits activity in wake-promoting populations including LDT/PPT (Rainnie et al. 1994), basal forebrain (Kalinchuk et al. 2008; Porkka-Heiskanen et al. 1997; Portas et al. 1997), and orexin neurons (Liu and Gao 2007). Furthermore, adenosine promotes activity in the sleep-promoting VLPO both indirectly (Chamberlin et al. 2003; Morairty et al. 2004) and, possibly, directly (Gallopin et al. 2005).

We modeled the homeostatic sleep drive through the variable h that increases during wakefulness and decreases during sleep states, reflecting extracellular adenosine concentrations. Because dissociated activity among wake-promoting populations may not be sufficient to initiate wakefulness (Gervasoni et al. 2000), the model criterion for wake depends on coordinated activity in the LC and DR. When the combined activity of both populations is sufficient to cross a threshold specified by θ_w, the network is in wake and the variable h increases toward 1; otherwise, the network is in sleep and h decreases to 0

$$h' = \mathrm{H}[(F_{\mathrm{LC}} + F_{\mathrm{DR}}) - \theta_w]\frac{(1-h)}{\tau_{hw}} - \mathrm{H}[\theta_w - (F_{\mathrm{LC}} + F_{\mathrm{DR}})]\frac{h}{\tau_{hs}} \quad (7)$$

where $H[z]$ is the Heaviside function defined as $H[z] = 0$ if $z < 0$, and $H[z] = 1$ if $z \geq 0$. The time scales of h growth (τ_{hw}) and decay (τ_{hs}) were chosen to generate physiological rat wake and NREM sleep bout durations. To incorporate this homeostatic sleep drive into the sleep-wake network model, we focused on the effects of adenosine on the VLPO. Because high adenosine concentrations were positively correlated with activity in the VLPO, we included an h dependence in the activation threshold of the model VLPO population (compare with *Eq. 2*)

$$F_{\mathrm{VLPO}\infty}(c) = VLPO_{\max}\,(0.5\{1 + \tanh[(c - \beta_{\mathrm{VLPO}}(h))/\alpha_{\mathrm{VLPO}}]\}) \quad (8)$$

where $\beta_{\mathrm{VLPO}}(h) = -kh$ with the parameter k relating the value of the homeostat to VLPO activation threshold.

For values of h near 1 (increased homeostatic sleep pressure), the VLPO activation threshold is at a low level so that the population is generally more excitable. This allows the VLPO to activate despite ongoing inhibition from the wake-promoting populations, thereby initiating the network transition to NREM sleep. For values of h near 0 (decreased homeostatic sleep pressure), higher VLPO activation thresholds prevent VLPO activation and allow the transition to wake.

In this sleep-wake regulatory network model, we simulated microinjection of GABA and ACh agonists and antagonists into the LC. Agonist and antagonist concentrations in the LC were modeled by *Eq. 4* ($i = G$ and A) and the endogeneous neurotransmitter concentrations in the LC were replaced with *Eq. 5* ($i = G$ and A, $X = LC$) for agonist microinjection simulations and with *Eq. 6* ($i = G$ and A, $X = LC$) for antagonist microinjection simulations. Numerical simulations of the network model were computed using a modified Euler method with time step 0.005 s implemented with the software XPPAUT, developed by G. B. Ermentrout and available at ftp://ftp.math.pitt.edu/pub/bardware.

RESULTS

Model captures realistic rat sleep-wake behavior

In simulations of the model network, states of wake, NREM sleep, and REM sleep were interpreted based on firing rates of neuronal populations. Neurotransmitter concentrations were closely correlated with firing rates of the associated presynaptic populations; thus each state was associated with high expression of the appropriate transmitters (Fig. 3). For example, wake was defined by activation of the wake-promoting populations (firing rates given by F_{LC}, F_{DR}, and F_{WR}) and high expression of NE, 5-HT, and ACh (concentration levels given by C_N, C_S, and $C_{A(WR)}$, respectively); NREM sleep was defined by activation of the VLPO (firing rate F_{VLPO}) and inactivation of wake-promoting populations, resulting in high GABA expression (concentration level given by C_G) and diminished monoamine and cholinergic expression; and REM sleep was associated with high F_{VLPO} levels and activation of the REM-promoting population (firing rate F_R) with its contribution to ACh expression (concentration level given by $C_{A(R)}$).

We obtained good agreement between the simulated sleep-wake behavior and experimentally reported baseline sleep-wake behavior for adult male Sprague-Dawley rats during the light period (Blanco-Centurion et al. 2007) using standard measures including total percentages of time in wake, NREM sleep, and REM sleep, mean bout durations, and numbers of bouts across 12 h (Fig. 4). Additionally, the general patterning of sleep and wake states matched those experimentally observed in the rat, including bidirectional transitions between wake and NREM sleep and transitions from NREM sleep to REM sleep followed by wakefulness (Weitzman et al. 1980). Both wake and NREM states showed large numbers of bouts with brief (<1 min) durations that are typical in the rat (Lo et al. 2004).

To understand how the network generates these stereotypical rodent sleep-wake patterns, we now discuss the key mechanisms that govern network state transitions. Wake bouts occurred as a result of two different effects. Brief wake bouts (Fig. 5*A*, upward arrows) were typically initiated by random excitatory inputs to the LC and DR populations. Because the neurotransmitter formalism introduces a slight time lag between the activation of LC/DR activity and the onset of full-strength NE/5-HT inhibition, these brief activations result in moderate levels of LC/DR activity and low levels of NE/5-HT release that, in turn, cause slight decreases in VLPO activation and GABA levels (see Fig. 3*C*, top 3 traces). Therefore brief activations of LC/DR can occur without a full transition of the network out of NREM sleep, and thus the model predicts that concurrent activity in wake- and sleep-promoting populations is possible for short periods of time.

Longer wake bouts were the result of a network transition to full LC and DR activation and maximal concentrations of NE and 5-HT, as well as activation of the cholinergic wake-promoting subpopulation of LDT/PPT. Full-strength monoaminergic inhibition to VLPO silenced VLPO activity and thereby reduced associated GABA release. These network transitions between wake and NREM sleep resulted from the homeostatic modulation of the VLPO activation threshold. As this threshold decreases during wake with the growth of the homeostatic sleep drive variable h, inhibition from wake-promoting populations is no longer sufficient to prevent VLPO activation, and the onset of activity in the VLPO initiates a transition from wake to NREM sleep (Fig. 5*A*). Similarly, transitions from NREM sleep to wake occur when recovery of the homeostatic sleep drive increases the VLPO activation threshold to terminate VLPO firing. When wake-promoting populations are re-

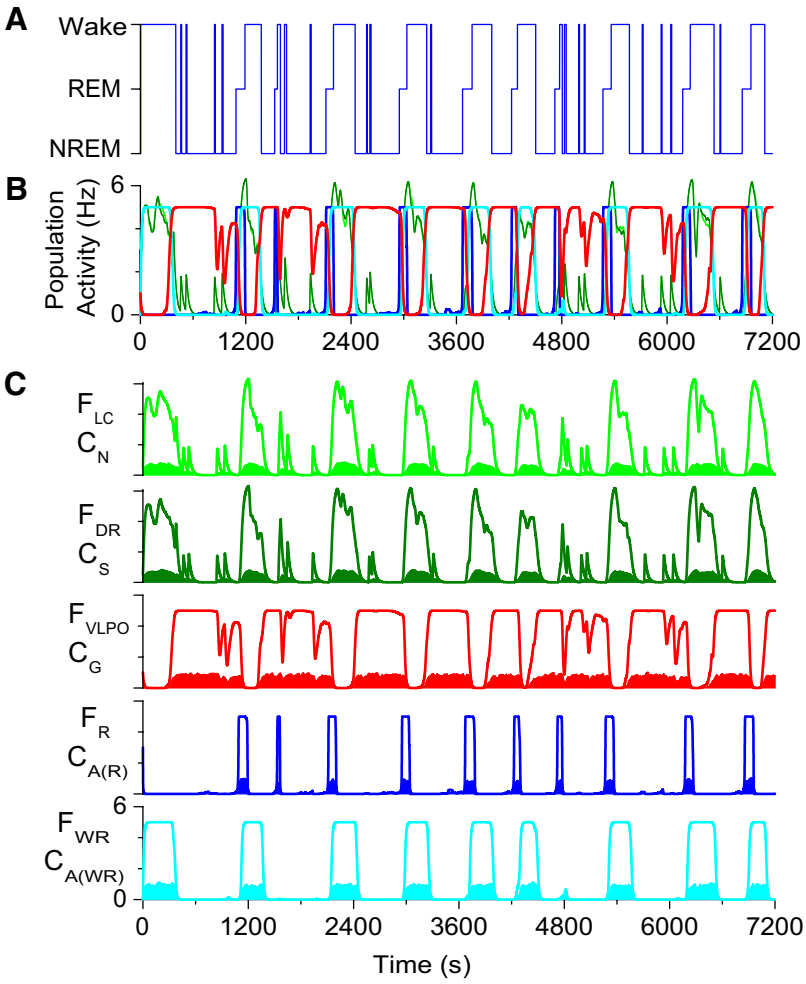

FIG. 3. Network model simulates rat sleep-wake behavior. *A*: hypnogram summarizing 2 h of simulated rat sleep-wake behavior (corresponding to data from the light period). *B*: state-dependent firing rates in wake-promoting populations LC ($F_{LC,}$ light green) and DR ($F_{DR,}$ dark green), NREM-promoting population VLPO (F_{VLPO}, red), REM- promoting population (F_R, blue), and wake/REM-promoting population (F_{WR}, light blue) determine the sleep-wake state recorded in the hypnogram. *C*: neurotransmitter concentrations C_i [i = N (NE), S (5-HT), G (GABA), A(R) (ACh expressed by REM-promoting population), and A(WR) (ACh expressed by wake/REM-promoting population)], shaded regions, track firing rates (in Hz, curves) in each associated presynaptic neuronal population (colors same as in *B*, see APPENDIX for parameter values).

leased from inhibition, the network transitions from NREM sleep to wake. This transition mechanism is consistent with the sleep-wake flip-flop conceptual model (Saper et al. 2001). In our model, this transition usually involves activation of the cholinergic REM-on population; thus the transition sequence is NREM sleep to REM sleep to wake.

Two separate mechanisms may initiate a transition from NREM sleep to REM sleep. One mechanism depends on the homeostatically driven transition from NREM sleep to wake. We can understand the details of this transition by considering network behavior in the absence of noisy components. In the deterministic network during the NREM state, activity in the sleep-promoting VLPO decreases as the homeostatic sleep drive recovers. The attenuation of VLPO inhibition to the REM-promoting LDT/PPT populations allows them to activate and initiate REM sleep. The combination of reduced inhibition from VLPO and increased excitation from LDT/PPT causes wake-promoting LC/DR to activate, thereby terminating the REM bout. This stereotypical and homeostatically driven pattern of NREM–REM-wake cycling corresponds to a stable periodic solution of the deterministic network (Fig. 5*B*) and is generally preserved in the noisy system.

The reliable activation of the REM-promoting population at the NREM sleep to wake transition is an inherent feature of the network structure. Periodic cycling in activation of the REM-promoting population, and LC and DR, similar to REM-on/REM-off oscillations in the reciprocal interaction model for REM sleep cycling (Massaquoi and McCarley 1992; McCarley and Hobson 1975), can occur in the network, but is not obtained for our default parameter values. The existence of this cycling pattern depends on the activation threshold of the REM-promoting population: cycling appears for low values of the threshold but not at higher values (Fig. 5*C*). While the default activation threshold does not permit this periodic cycling, the model trajectory is influenced by proximity to the periodic solution during the network transition from NREM sleep to wake. Therefore the REM-promoting population activates transiently despite ongoing inhibition as decreasing GABAergic inhibition from the VLPO is replaced by increasing monoaminergic inhibition from LC and DR.

The second mechanism for REM sleep initiation is related to noise in the network. Variability of neurotransmitter release results in varying levels of inhibition to and self-excitation by the REM-promoting population. If, during the NREM state, higher ACh release from the LDT/PPT populations is combined with lower levels of GABAergic inhibition, the model trajectory can be transiently attracted to the periodic REM-on/REM-off cycle described above (Fig. 5*A*, downward arrow). The wake bout after these spontaneous REM bouts is typically brief, and, while VLPO activation may be slightly inhibited, the network rarely transitions out of NREM sleep. During the wake state, this mechanism for REM sleep initiation is not

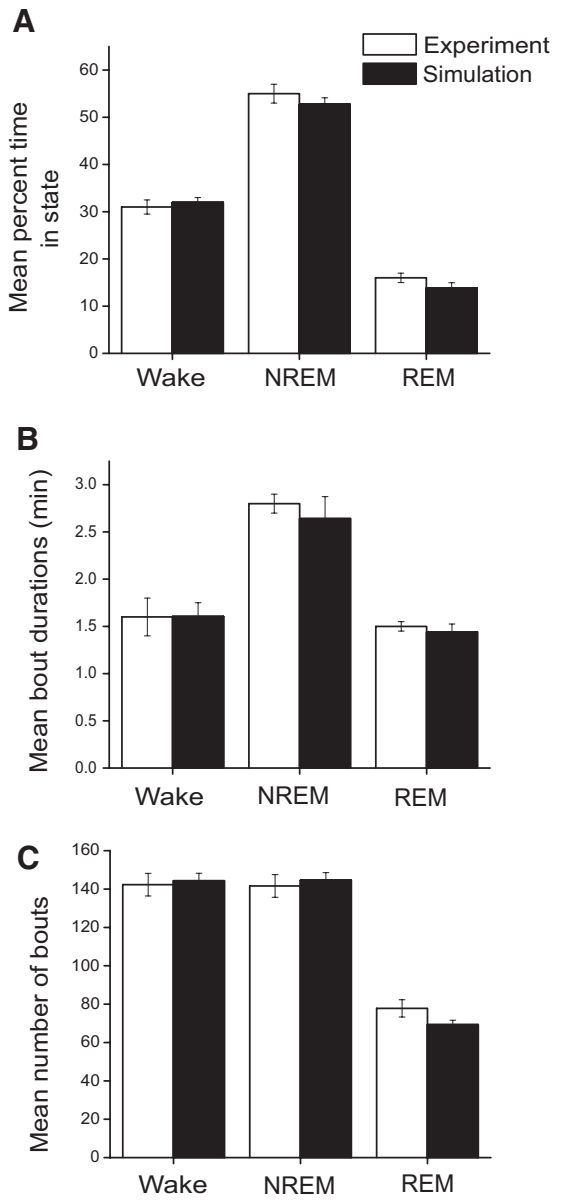

FIG. 4. Structure of simulated sleep-wake behavior is consistent with experimental data quantifying behavior of adult male Sprague-Dawley rats during the 12-h light period (Blanco-Centurion et al. 2007) as seen in the comparisons of the following standard measures. *A*: percent time spent in each state. *B*: mean bout duration. *C*: mean number of bouts over 12 h. Means and SD of model results determined from 10 simulation runs.

possible because high levels of LC/DR activation prohibit periodic cycling between the REM-promoting population and LC/DR. Thus this network structure never permits direct transitions from wake to REM sleep, consistent with experimental data (Benington and Heller 1994).

Model sensitivity to parameters

The model includes >60 parameters that describe intrinsic properties of neuronal populations (X_{max}, α_X, β_X, and τ_X for X = *LC, DR, R, WR*, and *VLPO*); intrinsic properties of neurotransmitters/neurotransmitter release [γ_i and τ_i for i = *N, S, A*(*R*), *A*(*WR*), and *G*]; coupling parameters ($g_{i,X}$); parameters governing the homeostatic sleep drive; parameters associated with noise; and parameters associated with simulated microinjections. Full parameter sets are given in the APPENDIX.

To evaluate model sensitivity to parameters, we performed simulations with each parameter varied by ±10% and assessed the effects on network behavior. In general, network behavior was robust to these variations of parameters (data not shown). The percent of total time spent in each state changed by less than ±8% as the result of variation in any of these parameters. Effects on mean bout durations and bout frequency were slightly more pronounced and typically reflected a loss of state consolidation associated with increases in bout frequency and decreases in mean

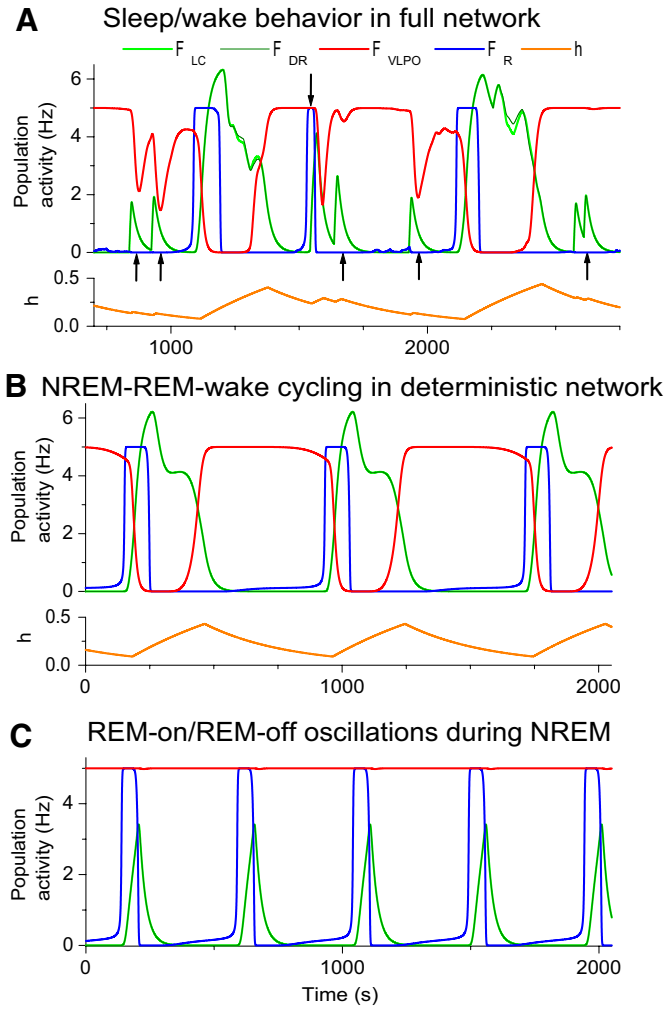

FIG. 5. Network mechanisms drive state transitions. *A*: approximately 30 min of 2-h simulation in Fig. 3*B* showing details of transitions in population firing rates (colors same as in Fig. 3). Brief awakenings (upward arrows) and spontaneous REM sleep (downward arrow) may occur during NREM sleep. The homeostatic sleep drive h (orange curve, *bottom panel*) increases during wake and decreases during sleep. *B*: in the deterministic network [$\delta(t) = 0$ and $\sigma_i(t) = 0$ for i = *N, S, G,* A(*R*) and A(WR), see APPENDIX for details], firing rates follow a regular cycle of NREM sleep–REM sleep-wake. Transitions between wake and NREM sleep are governed by the homeostatic sleep drive, h (orange curve, *bottom panel*), and its effect on the VLPO activation threshold. *C*: when F_{VLPO} activity is high and the activation threshold parameter for the REM-promoting population is in the appropriate range ($\beta_R = -0.51$, h set constant to 0.4), periodic cycling between activity in F_R and activity in F_{LC}/F_{DR} can occur. Although the default β_R parameter value ($\beta_R = -0.5$) does not correspond to the cycling regimen, the underlying dynamics of the full network are affected by their proximity to the periodic solution.

bout durations. Interestingly, increasing/decreasing a parameter did not necessarily result in reciprocal effects: often, both variations promoted fragmentation of behavioral states.

In addition to general parameter sensitivity, we investigated the importance of relative magnitudes among some sets of parameters. These relative differences often reflected physiological features of neuronal populations or neurotransmitter actions. For example, the ordering $\tau_{A(R)} = \tau_{A(WR)} = \tau_G < \tau_N = \tau_S$ reflects the faster action of ionotropic neurotransmitters ACh and GABA compared with the action of metabotropic NE and 5-HT (Destexhe et al. 1994). To determine the importance of these relative orderings, we ran simulations in which differences in intrinsic properties and differences in dynamics were systematically eliminated from modeled populations and neurotransmitters, respectively. To equalize population parameters, the slopes for the neuronal population steady-state functions were set to reflect fast ($\alpha_X = 0.25$) or slow ($\alpha_X = 0.75$) activation. To equalize parameters for time dynamics, the time constants for neuronal populations and neurotransmitter concentration were set to fast ($\tau_X = \tau_i = 10$ s) or slow scales ($\tau_X = \tau_i = 25$ s).

When representative parameters were used to ascribe equal properties to all populations and all neurotransmitters, the balance of time spent in wake and sleep was affected more substantially compared with changes observed under ±10% variations in parameters (data not shown). For example, when all populations were given equal slow properties and characteristics ($\tau_X = \tau_i = 25$ s; $\alpha_X = 0.75$; $\gamma_i = 4$), the percent time in wakefulness more than doubled. Typically, equal properties for populations and/or neurotransmitters caused an increase in percent time in wake and decrease in percent time in NREM sleep. These changes were caused by differences in both bout frequency and mean bout duration. Both increases and decreases in the percent time in REM sleep were observed, although there was a consistent decrease in REM bout duration, regardless of whether the parameters specified fast action or slow action. These results indicate that maximal REM bout durations are obtained in our network structure when parameters dictating dynamic properties of populations and transmitters differ in their relative magnitudes.

Simulation of GABA agonist/antagonist microinjection in the LC

Simulated microinjection of GABA agonist and antagonist into the LC had a robust effect on REM sleep by producing increases and decreases, respectively, in total REM sleep and REM bout duration in the 4 h after microinjection (Fig. 6). These effects were consistent with microinjection experiments (Mallick et al. 2001). To determine the mechanism responsible for the changes in REM bout duration, we analyzed microinjection simulations in the deterministic model (Fig. 7). In the control case, REM bouts were terminated by the onset of inhibition to the REM-promoting population from coordinated activity in LC and DR. In the presence of microinjected GABA agonist, LC is tonically inhibited. Therefore firing in the DR precedes firing in the LC and lasts longer before triggering a transition to wake. The combined reduction in LC activity and LC/DR coordination results in a longer mean REM bout duration (Fig. 7*B*). Conversely, in the presence of a GABA antagonist, tonic inhibition to the LC is reduced. This allows strong anticipatory firing in the LC, which precedes activity in the DR and increases combined LC/DR inhibition, thereby accelerating REM bout termination (Fig. 7*C*). Thus the LC activation profile modulates changes in REM bout duration. With the addition of noise in the full system, this mechanism was preserved.

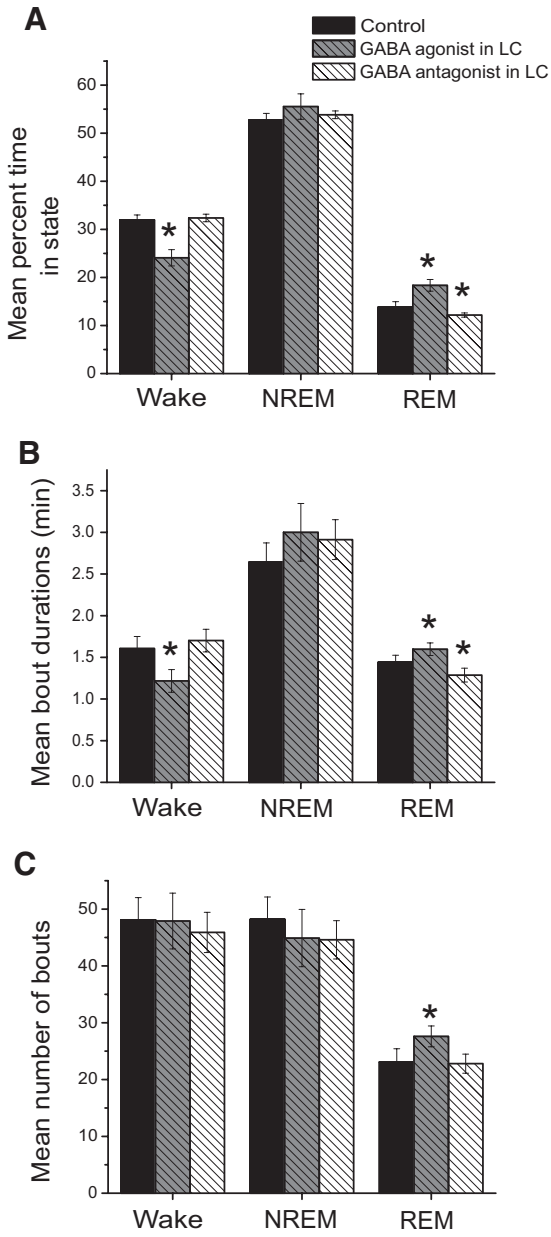

FIG. 6. Microinjection of GABA agonist/antagonist into LC alters the structure of simulated sleep-wake behavior. All results are reported for the 4 h after simulated microinjection. *A*: microinjection of the GABA agonist/antagonist increase/decrease, respectively, the percent time in REM sleep. With the GABA agonist, there is also a tendency toward an increase in NREM sleep, which comes at the expense of time in wakefulness. *B*: increased/decreased mean REM bout durations contribute to the effects on percent time in REM sleep. In addition, the GABA agonist-induced decrease in time spent in wakefulness is caused by a decrease in mean wake bout duration. *C*: microinjection of GABA agonist also increases the number of REM bouts. [Initial condition for GABA agonist simulation $P_G(0) = 2.0$ and for GABA antagonist simulation $Q_G(0) = 1.0$; see APPENDIX for details. Means and SD of model results determined from 10 simulation runs; $^*P < 0.01$ in ANOVA with control data.]

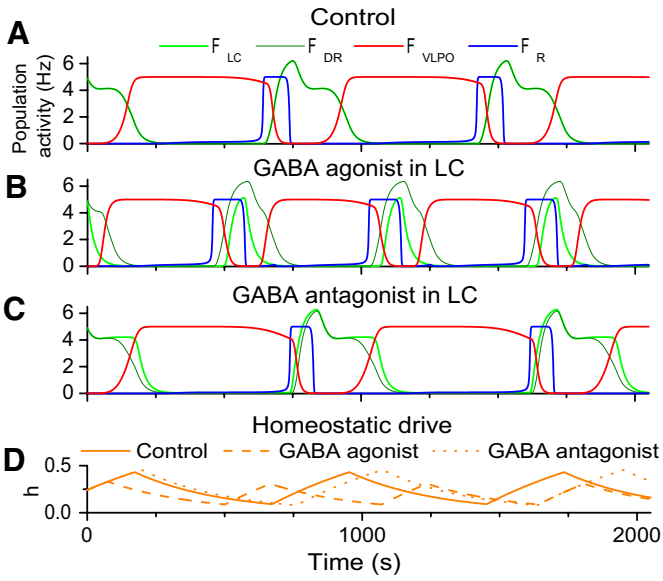

FIG. 7. The effect of simulated GABA agonist/antagonist in the LC on REM bout duration is mediated by changes in LC activation, shown in the deterministic network [$\delta(t) = 0$ and $\sigma_i(t) = 0$ for $i = N, S, G$, A(R) and A(WR), see APPENDIX for details]. *A*: under control conditions, activation of F_{LC} (light green) and F_{DR} (dark green) is synchronized. Inhibition from these populations terminates activity of F_R (blue) resulting in the end of the REM bout (F_{VLPO}, red). *B*: in the presence of a GABA agonist in the LC, F_{LC} activation is delayed compared with F_{DR}. This prolongs activation of F_R, thereby increasing mean REM bout duration. *C*: in the presence of a GABA antagonist in the LC, F_{LC} activation anticipates activation of F_{DR}. Therefore F_R activation is terminated more quickly and mean REM bout durations are decreased. *D*: in addition to the immediate effect on REM bout duration, microinjections affect overall cycle length. The oscillation of homeostatic sleep drive h (orange curves) reflects the GABA agonist (dashed)/antagonist (dotted)-induced decrease/increase compared with control (solid).

In addition to the effects on REM sleep, changes in the LC activation profile under simulated microinjection of GABA agonist also affected mean wake bout durations (Fig. 6*B*). Again, we turn to the deterministic model to understand this effect (Fig. 7). In the presence of the GABA agonist, tonic inhibition to LC reduced LC firing rates during wake, thereby reducing the level of noradrenergic inhibition of VLPO. This reduction in inhibition allowed VLPO to activate and truncate wakefulness at lower activation thresholds compared with its baseline behavior. Because the VLPO activation threshold varies inversely with the homeostatic sleep drive variable h, this change in activation threshold is reflected in the decreased h peak value at the transition from wake to NREM sleep (Fig. 7*D*, dashed curve). Conversely, in the presence of the GABA antagonist, wake bouts are extended because LC activity and associated noradrenergic inhibition to VLPO remain higher during wakefulness, and the VLPO activation threshold must decrease to lower than normal levels to allow VLPO activation. This is reflected in the slightly higher peak value of h at the wake to NREM sleep transition (Fig. 7*D*, dotted curve).

These changes in the homeostatic regulation of the VLPO activation threshold can also affect mean NREM bout durations: when the VLPO activation threshold necessary to terminate a wake bout is lower or higher compared with control, the subsequent recovery of the threshold is longer or shorter, respectively. Thus the shorter wake bouts associated with the GABA agonist cause shorter subsequent NREM bouts and the period of the homeostatically regulated cycle of NREM sleep-REM sleep-wake is decreased (Fig. 7*B*); this decrease in cycle length results in an increased frequency of wake, NREM, and REM bouts under these conditions. Similarly, the presence of a GABA antagonist increases the period of the cycle and decreases the frequency of wake, NREM sleep, and REM sleep bouts (Fig. 7*C*).

However, these changes in wake and NREM bout duration and number of bouts are not reflected in the full model in the presence of noise (Fig. 6). Most notably, in the full model under GABA agonist microinjection, mean wake bout durations are decreased, as predicted by the deterministic model, but mean NREM bout durations tended to increase. This contrast with behavior in the deterministic system occurs because other mechanisms for LC activation are affected by the microinjection. In this case, the GABA agonist tonically inhibits LC and attenuates its response to random excitatory inputs. Thus the combined LC/DR response may not be sufficient to induce a brief wake bout, and the number of short wake bouts can decrease in these simulations (see Fig. 9*B*, middle traces). As a result, NREM bouts continue uninterrupted by brief wakes, which results in increased mean NREM bout durations. As the injected GABA agonist levels decay, LC responses to the random excitatory inputs recover, and brief wake bouts are able to interrupt NREM sleep. Thus the number of wake and NREM bouts over the full 4 h does not differ significantly from control despite transient changes. However, the shortened cycle length of the deterministic model is reflected in the increase in the number of REM bouts. Under simulated GABA antagonist, overall levels of inhibition to LC during NREM sleep are lower, and brief wakes occur as in control conditions. However, the changes in the homeostatically regulated NREM sleep-REM sleep-wake cycle discussed above are reflected in the slight increases in wake and NREM bout durations and slight decreases in bout frequency.

In summary, changes in LC activation levels induced by simulated microinjection of GABA agonist and antagonist directly affected both wake bout duration, because the LC is one of the primary wake-promoting populations, and REM bout duration, because LC activity influences activation of the REM-promoting population. These changes also affected the mean percent time spent in states of wake and REM sleep. The change in wake bout duration can be propagated through the network to affect the homeostatic drive and NREM bout duration, as observed in the deterministic model. In the full model in the presence of noise, simulated microinjection of GABA agonist and antagonist induced opposite effects on percent time in REM sleep and mean REM durations, but a presumed agonist/antagonist reciprocal action was not observed for wake and NREM states because of multiple mechanisms for LC activation in the network.

Simulation of ACh agonist/antagonist microinjection in the LC

Simulated microinjection of cholinergic agonist and antagonist in the LC also resulted in widespread effects on sleep-wake architecture for the 4 h after microinjection (Fig. 8). Many of these effects reflected mechanisms linked to LC activation and paralleled changes elicited by simulated GABA antagonist and agonist microinjection. For example, simulated microinjection of ACh agonist in the LC caused a decrease in mean REM bout duration similar to that observed with simu-

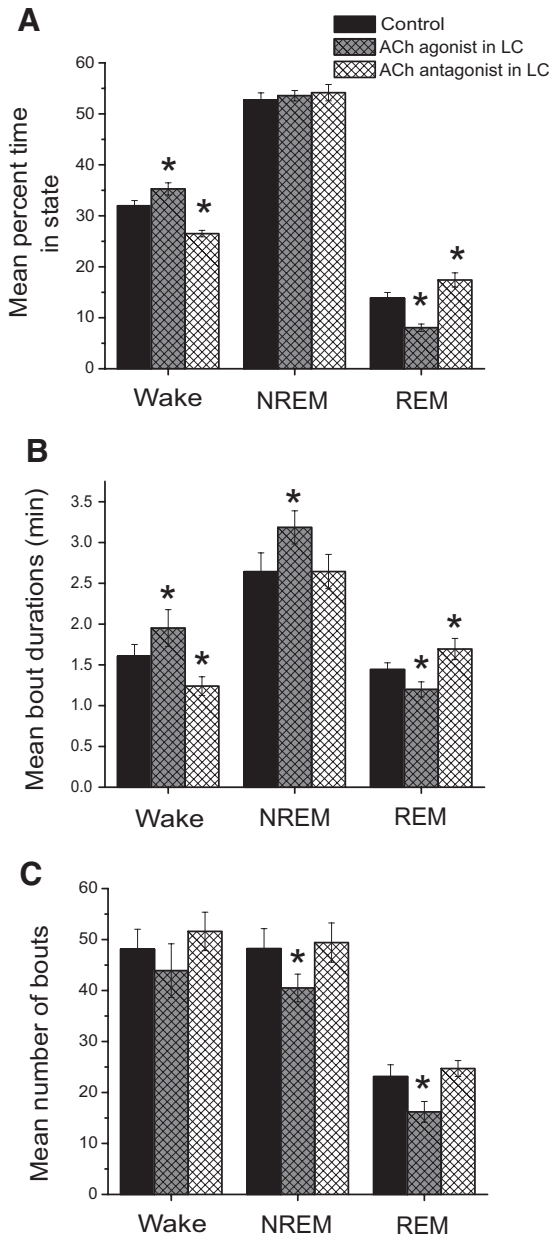

FIG. 8. Microinjection of ACh agonist/antagonist into LC alters the structure of simulated sleep-wake behavior. All results are reported for the 4 h after simulated microinjection. *A*: microinjection of ACh agonist/antagonist decreased/increased the percent time spent in REM sleep. Reciprocal changes were observed in the percent time spent in wake. *B*: changes in mean wake and REM bout durations contributed to the changes in time spent in these states. In addition, mean NREM bout durations were increased in the presence of the ACh agonist. *C*: in the presence of the ACh agonist, the number of NREM and REM bouts was decreased. [Initial condition for ACh agonist simulation $P_A(0) = 0.8$ and for ACh antagonist simulation $Q_A(0) = 0.55$; see APPENDIX for details. Means and SD of model results determined from 10 simulation runs; $*P < 0.01$ in ANOVA with control data.]

lated microinjection of GABA antagonist, and these decreases can be attributed to a similar mechanism: higher LC activity accelerates LC activation at the REM sleep-wake transition, which truncates the REM bout and extends the wake bout. The propagated effects of a longer wake bout on the homeostatic sleep drive and NREM bout duration led to an increase in NREM bout duration and a decrease in the number of NREM bouts. Likewise, the changes to REM and wake bout durations caused by simulated ACh antagonist in the LC are similar to those of simulated GABA agonist microinjection. Specifically, mean REM bout duration is increased because reduced cholinergic excitation to LC attenuates NE inhibition to the REM-promoting population, thus requiring higher levels of coordinated LC/DR activity to terminate the REM bout. Mean wake bout duration is decreased because reduced LC activity levels reduce NE inhibition to the VLPO and allow earlier VLPO activation to truncate wake bouts.

Despite these similarities, ACh agonist/GABA antagonist and ACh antagonist/GABA agonist pairs may exert different effects across sleep-wake states because neurotransmitter agonists affect sleep-wake behavior in all states, whereas antagonists act only when the appropriate state-dependent neurotransmitter is present. For example, the reduction in REM frequency caused by the microinjected cholinergic agonist was not observed under microinjected GABA antagonist. In the presence of ACh agonist, LC receives tonic excitatory input that prevents complete termination of its activity during the NREM state and sustains its inhibitory input to the REM-promoting population. This maintained inhibition suppressed both spontaneous REM bouts and activation of the REM-promoting population at the homeostatically regulated transitions out of NREM sleep. Thus the number of REM bouts was very low for the first hour of the simulation (Fig. 9*A*). As the level of injected ACh agonist decayed, the number of REM bouts recovered to levels closer to control. In contrast, simulated GABA antagonist microinjection did not significantly affect the number of REM bouts.

This difference between tonic activity of an injected agonist and state-dependent activity of an injected antagonist is also evident in the simulated ACh antagonist microinjections. Simulated ACh antagonist microinjections do not affect brief wake bouts because the random, excitatory inputs to LC are not presumed to be cholinergically mediated. Therefore in contrast to simulated GABA agonist microinjections, brief wakes persist under simulated ACh antagonist conditions (Fig. 9*B*). In the figure, probability density functions for wake bout durations show peaks at short durations (<1 min) for the control and simulated ACh antagonist microinjections, especially in the second to fourth hours of the simulations (*top* and *bottom*). This peak is notably absent in the probability density functions for the first to third hours of the simulated GABA agonist (*middle*) but reappears in the fourth hour as the effect of the simulated agonist dissipates and brief wakes resume. As a result of the maintenance of brief wakes under simulated ACh antagonist conditions, NREM bout durations in this condition are not affected, even though, through the mechanisms of the deterministic model, shorter wake bouts act to reduce NREM bout durations. The influence of shorter wake bouts in the deterministic model on wake bout durations in the noisy model is shown by the shift of the secondary lower peaks to shorter durations in the simulated GABA agonist and ACh antagonist simulations (*middle* and *bottom*) compared with the control case (*top*, vertical line indicates the mean wake bout duration in the deterministic model).

In summary, many of the effects of changes in LC activation levels by simulated microinjection of ACh agonist and antagonist mirror those of simulated GABA antagonist and agonist, respectively. Exceptions can be attributed

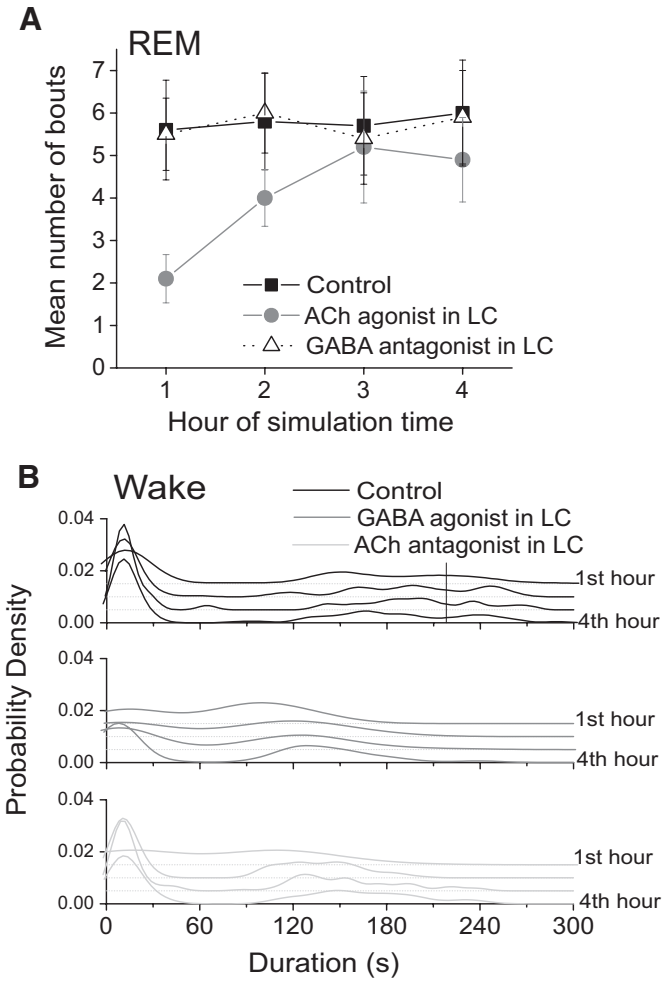

FIG. 9. ACh agonist/GABA antagonist and ACh antagonist/GABA agonist pairs show differences in their effects on sleep-wake behavior. Furthermore, the dynamics of microinjected agonist/antagonist decay alter their effects on sleep-wake behavior over time. *A*: simulated microinjection of ACh agonist into the LC results in an initial decrease in REM frequency that is not observed with microinjection of a GABA antagonist. This decrease is attenuated as the ACh agonist decays over time. *B*: probability density functions describe changes in the distribution of wake bout durations over 4 h in control conditions (*top*) and after simulated microinjection of GABA agonist (*middle*) and ACh antagonist (*bottom*) in the LC. Each trace denotes the probability density for 1 h of wake bout duration data with the progression from *top* to *bottom* corresponding to hours 1, 2, 3, and 4 after the simulated microinjection. In each panel, the top 3 traces have been vertically offset for clarity. The vertical line in the control panel denotes the mean wake bout duration in the deterministic model when noisy components are absent [$\delta(t) = 0$ and $\sigma_i(t) = 0$, APPENDIX for details], showing the influence of dynamics in the deterministic model on the noisy model. Under simulated GABA agonist (*middle*), the absence of a peak at short durations (<1 min) in probability densities in the 1st to 3rd h reflects a suppression of brief wake bouts that does not occur with simulated microinjection of ACh antagonist (*bottom*). (Model data same as in Figs. 6 and 8.)

to the difference in the state dependence or independence of action of an injected agonist and antagonist. Specifically, sustained LC activity during NREM sleep under simulated microinjection of ACh agonist caused a significant reduction in the number of REM bouts that did not occur with the simulated GABA antagonist. Additionally, simulated ACh antagonist did not affect the efficacy of the random, excitatory inputs to the LC to induce brief wakes, unlike simulated GABA agonist.

Model prediction for modulation of REM frequency but not duration

Despite the expected parallels between ACh agonist/GABA antagonist and ACh antagonist/GABA agonist pairs, simulation results for cholinergic agonists/antagonists contrasted with experimental observations. One inconsistency was that experimental microinjection of cholinergic agonists/antagonists into the LC significantly affected frequency of REM bouts with less influence on REM bout duration (Mallick et al. 2001). The discrepancies between these results and our simulations suggest that REM sleep control may not be a direct result of LC activity and are further addressed in the DISCUSSION. However, as a first step in revising network structure/interactions, we analyzed the network behavior to identify mechanisms that affected the frequency of REM sleep without affecting mean REM bout duration.

The primary mechanism that satisfied these criteria was modulation of the activation threshold β_R for the steady-state firing rate function of the REM-promoting population, $F_{R\infty}(\cdot)$. Lower activation thresholds increased REM frequency and higher activation thresholds decreased REM frequency without altering mean REM bout duration (Fig. 10). Similar changes were observed in the number of wake and NREM bouts caused by an overall change in cycle length. Although mean REM and wake bout durations were not affected, the altered frequency of REM bouts resulted in changes to fragmentation of NREM sleep and associated changes in mean NREM bout durations. Increases or decreases in the frequency of NREM bouts did not compensate for the changes in mean NREM bout durations as reflected by the altered total amounts of NREM sleep. These results suggest that initiation of REM sleep results from direct modulation of activation in REM-promoting populations while maintenance of REM sleep can be governed by network dynamics.

DISCUSSION

In this study, we introduced a novel modeling framework for investigating the structure and dynamics of sleep-wake regulation. The model simulates realistic rat sleep-wake behavior and the modulation of this behavior with microinjection of GABAergic and cholinergic agonists/antagonists into one of the key wake-promoting populations. Furthermore, detailed analysis of network dynamics provides insights into the mechanisms underlying agonist/antagonist modulation of baseline behavior.

Advantages and limitations of the modeling formalism

In our firing rate formalism, we allow for the time evolution of both the postsynaptic response to total input and the total input in response to presynaptic population activity. Most firing rate models assume that one of these processes is instantaneous; either setting firing rate equal to the steady-state firing rate function (Deco et al. 2008; Phillips and Robinson 2007, 2008; Steyn-Ross et al. 2005; Wilson et al. 2005, 2006) or setting total input as the weighted sum of all presynaptic firing rates (Wilson and Cowan 1972) (also reviewed in Ermentrout 1998). Of those models that allow for time dynamics of total input, some consolidate the dynamics of all presynaptic sources under one time constant (Phillips and Robinson 2007, 2008), whereas others, similar to our formalism, allow for

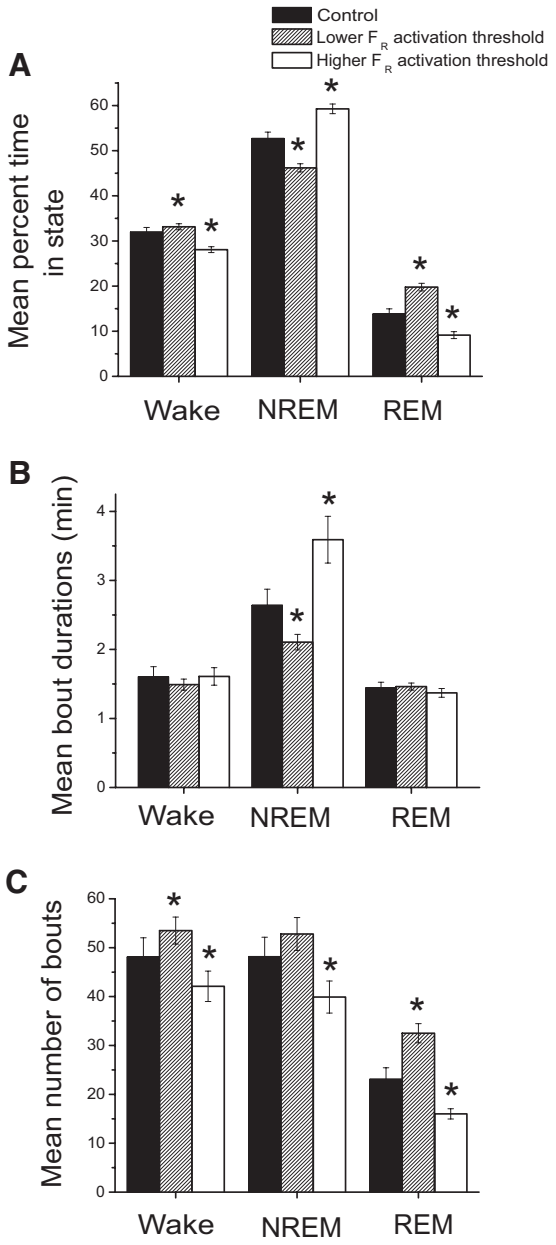

FIG. 10. Changes in the activation threshold β_R of the steady-state firing rate function for the REM-promoting population, $F_{R\infty}$ affect the frequency of REM bouts but not their duration. *A*: lower ($\beta_R = -0.6$) and higher ($\beta_R = -0.42$) thresholds result in increased and decreased, respectively, time spent in wake and REM sleep at the expense of NREM sleep compared with control ($\beta_R = -0.5$). *B*: the mean bout durations of NREM sleep were decreased/increased by lowering/raising thresholds, but bout durations of other states were not affected. *C*: with the lower threshold, increased numbers of wake and REM bouts were responsible for the change in percent time spent in these states. Similarly, with the higher threshold, a decrease in the number of REM bouts contributed to a decrease in the percent time spent in REM sleep. However, the higher threshold was also associated with a decrease in the number of NREM bouts, which was not sufficient to compensate for the increase in mean NREM bout duration. (Means and SD of model results determined from 10 simulation runs; $^*P < 0.01$ in ANOVA with control data.)

distinct time constants for each presynaptic source (Steyn-Ross et al. 2005; Wilson et al. 2005, 2006) (also reviewed in Deco et al. 2008). We find that explicit consideration of the dynamics of presynaptic sources, or neurotransmitter concentrations in our formalism, introduces flexibility that is necessary to capture the complexity of the system. Specifically, the inclusion of neurotransmitter dynamics can describe the biophysical variability inherent in population interactions. In addition, in our model dynamics, network transition mechanisms are preserved in the presence of noisy input. For example, because mutual inhibition between wake- and sleep-promoting populations is mediated through their associated neurotransmitters, transient activation of wake-promoting populations can occur without inducing a full network transition to wakefulness.

A distinct advantage of modeling individual neurotransmitter dynamics is the ability to directly incorporate data from microdialysis and microinjection experiments into the modeling formalism. Tamakawa et al. (2006) simulated several pharmacological microinjection experiments to help to constrain their choice of sleep-wake network model structure. However, their simulations involved static changes to parameters associated with activity in the target populations and did not address the dynamic properties of the microinjection, such as decay of the injected agents or effects on physiological transmitter release. Furthermore, because the changes were global and constant throughout the simulation, they could not consider the state-dependent action of microinjected neurotransmitter antagonists. In our simulations, agonists persist in the network during all states, so every state and state transition may be affected by their presence. In contrast, antagonists exert an effect only when the relevant neurotransmitter is present. Because the presence of specific neurotransmitters in these populations is state dependent, this implies that antagonists directly affect only a subset of states and state transitions. By explicitly modeling neurotransmitters, we can incorporate microinjection experiments in a dynamic, physiologic framework while analyzing the action of agonists and antagonists. Finally, while we concentrated on simulating microinjection experiments in this study, our formalism allows simulation of different techniques for administration of pharmacological agents to brain regions. As an example, microdialysis administration of a neurotransmitter agonist can be simulated by slow increases of the agonist variable $P_i(t)$ and of the scaling factor of endogenous release $m_i(t)$ to saturating levels reflecting the equilibration of the agent in the perfusion fluid in the dialysis probe (Watson et al. 2006).

Despite these advantages, this formalism does have several limitations. The main limitation is the sparse data pertaining to the dynamics of neurotransmitter release on a population scale. Although we have inferred appropriate time scales from dopamine voltammetry experiments (Garris and Wightman 1994), current limitations in experimental techniques make it difficult to establish appropriate dynamics for the neurotransmitters involved in sleep-wake regulation. Furthermore, this formalism is subject to the limitations of all firing-rate models. In particular, it assumes that population activity can be modeled with a single average firing rate: populations with heterogeneous intrinsic properties may need more complex steady-state firing profiles or may even need to be modeled with multiple firing-rate models as with the REM- and wake/REM-promoting subpopulations of LDT/PPT. Current experimental data indicate that our assumptions of averaged firing rates are reasonable, but these assumptions must be constantly re-evaluated in the face of new experiments.

Comparison with experimental results

Mallick et al. (2001) studied the effects of microinjection of GABAergic and cholinergic agonists and antagonists into LC in Wistar rats. They found that microinjection of GABA increased total REM sleep by increasing mean REM bout durations, whereas microinjection of the GABA antagonist picrotoxin had the opposite effect. They also noted that the GABA and picrotoxin microinjections increased and decreased, respectively, time in active waking with compensatory changes in slow wave sleep; changes in frequency or mean duration of these states were not reported.

Because of differences between our control dataset (Blanco-Centurion et al. 2007) and the control data reported by Mallick and colleagues, possibly because of the use of different rat strains, we could not quantitatively compare our results. However, we qualitatively compared the overall trends on sleep-wake patterning observed in our simulations with the differences they identified. Although our results regarding changes in REM sleep were consistent with data reported by Mallick and colleagues, our simulations showed opposite effects on wake and NREM sleep. Because wake-promoting LC neurons are under tonic GABAergic inhibition (Kawahara et al. 1999), it is surprising that increases in GABAergic inhibition increase wakefulness. One possible explanation of this apparent contradiction involves the mechanism for sleep homeostasis. In our model, the variable h associated with sleep homeostasis increases during wake and decreases during sleep with constant rates such that the amount of change is dependent on the time spent in each state. However, if the rate of increase and decrease depended on factors such as LC activity, the lower levels of activity caused by GABA microinjection may translate to an extension of wake bouts. In future work, a refined, dynamic sleep homeostat could be used to explore this potential mechanism.

Mallick et al. (2001) also found that microinjection of the cholinergic agonist carbachol in the LC increased total REM sleep by increasing the frequency of REM sleep and that microinjection of the cholinergic antagonist scopolamine decreased REM sleep by decreasing the frequency of REM initiation. There were trends toward increased/decreased REM bout durations with carbachol and scopolamine, respectively, but these differences were not significant. They did not report any changes to other behavioral states.

Our simulations of cholinergic agonist and antagonist microinjections showed opposite effects on total REM sleep and primarily attributed these changes to differences in mean bout duration, although simulated cholinergic agonist did affect mean number of REM bouts. Our results are consistent with experiments in cats (Masserano and King 1982; Vanni-Mercier et al. 1989), suggesting that the role of cholinergic agonists/antagonists in the regulation of REM sleep may differ between species. Apparent species differences may also be caused by the challenge of localizing microinjections in the small rodent brain (Brown et al. 2006), or they may reflect a limitation in the current model structure. Alternatively, the net effect of a cholinergic agonist on LC population activity may not be purely excitatory given the presence of local GABAergic cells within the LC (Iijima and Ohtomo 1988) and different muscarinic cholinergic receptor subtypes on LC cells (Baghdoyan 1997). In vitro studies have identified an excitatory effect of activation of M2 muscarinic receptors in the LC (Egan and North 1985), but inhibitory actions of other receptor subtypes have been indicated in nearby pontine structures (Egan and North 1986; Gerber et al. 1991). The discrepancies between model and experimental results suggest that variations in network structures for REM regulation should be considered, and they highlight the utility of formal mathematical modeling for constraining conceptual models.

Probing the mechanisms for REM sleep generation

Recent experimental evidence has challenged the cholinergic hypothesis for REM sleep regulation in rodents, and several competing conceptual models of REM sleep regulation have been proposed. Because GABA is the neurotransmitter responsible for the slowing and eventual cessation of activity in the DR and LC that gates the production of REM sleep (Gervasoni et al. 1998; Nitz and Siegel 1997), these models focus on the importance of recently identified REM-active GABAergic populations (Brown et al. 2008; Lu et al. 2006; Luppi et al. 2006; Sapin et al. 2009) and attribute to the cholinergic system varying levels of involvement in REM sleep initiation and maintenance.

Several groups have suggested modifications of the reciprocal interaction model in which LC/DR and LDT/PPT act on intermediate GABAergic populations that ultimately control different aspects of REM sleep. In the cellular-molecular-network (CMN) model of REM sleep proposed by Datta and MacLean (2007), ACh from LDT/PPT promoted activity in populations involved in specific aspects of REM sleep, termed REM sleep-sign generators. Simultaneously, local GABAergic populations inhibited LC and DR to facilitate disinhibition of the REM sleep-sign generators. Hence, the roles of these generators in governing specific REM sleep signs were reconciled with significant roles for LC/DR and LDT/PPT. Mallick et al. (2001) also invoked the presence of local GABAergic populations in LC and DR. They suggested that the counterintuitive effects of microinjected cholinergic agonists/antagonists in the LC on REM sleep were caused by local GABAergic mediation of standard cholinergic effects (Mallick et al. 2001). This hypothesis highlights the importance of considering mechanistic differences between the effects of endogenous and exogenous neurotransmitter.

Other groups have rejected the cholinergic hypothesis altogether. Lu et al. (2006) proposed that control of REM sleep is achieved through a REM-on/REM-off flip-flop switch resulting from reciprocal GABAergic inhibition between REM-on neurons in the sublaterodorsal nucleus (SLD) and precoeruleus (PC) and REM-off neurons in the ventrolateral part of the periaqueductal gray matter (vlPAG) and lateral pontine tegmentum (LPT). They noted that LC/DR and LDT/PPT may help to modulate REM sleep, but they did not consider these populations to play essential roles in the circuitry. Luppi and colleagues have proposed that the vlPAG is the most important structure for REM control and that vlPAG contains both REM-on and REM-off neurons (Luppi et al. 2006; Sapin et al. 2009). Local interactions within the vlPAG, as well as interactions with other GABAergic and monoaminergic structures, govern transitions into REM sleep.

McCarley and colleagues suggested a conceptual model that incorporates both cholinergic and GABAergic mechanisms in

the control of REM sleep (Brown et al. 2008). In their proposed model, there is mutual GABAergic inhibition between REM-on neurons in the subcoeruleus and pontine nucleus oralis and REM-off neurons in the LPT, and ACh excites the REM-on neurons and inhibits the REM-off neurons. This provides essential cholinergic modulation of the GABAergic flip-flop structure. Furthermore, because the REM-on GABAergic neurons in subcoeruleus inhibit the LC and DR, indirect reciprocal interaction between monoaminergic and cholinergic populations continues to play a role in this conceptual model of REM sleep regulation.

Although these conceptual models specify the roles of different populations during REM sleep and the projections that cause or reinforce these state-dependent behaviors, they rarely account for mechanisms of transition in and out of REM sleep. In addition, conceptual models often fail to address mechanisms for the regular alternation between NREM and REM sleep that is a feature of normal sleep in several species including humans (Carskadon and Dement 2000). It has been difficult to establish similar periodicity in the polyphasic sleep-wake behavior of rodents. However, if the mechanisms for generating REM sleep are similar across species, the structure of a REM sleep generating network should suggest a basis for NREM-REM periodicity. Dynamic mathematical modeling of the REM-on/REM-off flip-flop switch suggested that both inhibition from the VLPO cluster to the extended VLPO and a drop in extended VLPO activity before sleep onset were necessary to achieve NREM-REM alternation (Rempe et al. 2009), but physiological support for these predictions has not yet been established. However, NREM-REM alternation was an important feature of the McCarley-Hobson reciprocal interaction model (Massaquoi and McCarley 1992; McCarley and Hobson 1975). Although the control parameter regimen (describing rat sleep-wake behavior) for our model did not produce regularly occurring NREM-REM alternation, our network structure admits a similar periodic mechanism.

Control of REM sleep must be understood in the larger context of the regulation of sleep-wake behavior. However, it can be difficult to infer the state-dependent dynamics that result from a given conceptual model. Therefore formal dynamic modeling approaches complement ongoing experimental studies to evaluate proposed network structures and shape our understanding of REM sleep regulation.

APPENDIX

Simulation results in Figs. 3–10 were obtained with equations and parameter values given here except where noted below and in the figure captions. When possible, parameter values were based on experimental data. When such data were unavailable, we chose parameters that were consistent with available experimental characterizations of neuronal populations, neurotransmitter actions, and the state-dependent behavior we expected from the network. Additional details are provided below.

For each neuronal population, the postsynaptic firing rate, $F_X(t)$ (in Hz, $X = LC, DR, VLPO, R,$ or WR), is governed by an equation of the following form

$$F'_X = \frac{F_{X\infty}\left(\sum_i g_{i,X}\, C_i\right) - F_X}{\tau_X} \tag{9}$$

where the steady-state firing rate $F_{X\infty}(\cdot)$, is a saturating function, its argument is summed over the neurotransmitters [i = norepinephrine (N), serotonin (S), GABA (G), or acetylcholine (A)] released to the postsynaptic population X, the $g_{i,X}$ are constant weights, and τ_X is the time constant associated with the response dynamics of the postsynaptic population. The individual equations for each population are given by the following

$$F'_{LC} = \frac{F_{LC\infty}[g_{A,LC}\, C_A - g_{N,LC}\, C_N - g_{G,LC}\, C_G + \delta(t)] - F_{LC}}{\tau_{LC}} \tag{10}$$

$$F'_{DR} = \frac{F_{DR\infty}[g_{A,DR}\, C_A - g_{S,DR}\, C_S - g_{G,DR}\, C_G + \delta(t)] - F_{DR}}{\tau_{DR}} \tag{11}$$

$$F'_{VLPO} = \frac{F_{VLPO\infty}(-g_{N,VLPO}\, C_N - g_{S,VLPO}\, C_S - g_{G,VLPO}\, C_G) - F_{VLPO}}{\tau_{VLPO}} \tag{12}$$

$$F'_R = \frac{F_{R\infty}(g_{A,R}\, C_A - g_{N,R}\, C_N - g_{S,R}\, C_S - g_{G,R}\, C_G) - F_R}{\tau_R} \tag{13}$$

$$F'_{WR} = \frac{F_{WR\infty}(g_{A,WR}\, C_A - g_{G,WR}\, C_G) - F_{WR}}{\tau_{WR}} \tag{14}$$

The constant weights $g_{i,X}$ are given by

$g_{A,LC}$,	3.5;	$g_{G,DR}$,	1.5;	$g_{A,WR}$,	1;
$g_{N,LC}$,	1.5;	$g_{A,R}$,	2.5;	$g_{G,WR}$,	1.7;
$g_{G,LC}$,	1.5;	$g_{N,R}$,	3.5;	$g_{N,VLPO}$,	2;
$g_{A,DR}$,	3.5;	$g_{S,R}$,	3.5;	$g_{S,VLPO}$,	2;
$g_{S,DR}$,	1.5;	$g_{G,R}$,	1.25;	$g_{G,VLPO}$,	0.5

and were chosen to produce appropriate steady-state behavior in each postsynaptic population during wake, NREM sleep, and REM sleep. For example, because VLPO has a sleep-active firing profile, the parameters $g_{N,VLPO}$ and $g_{S,VLPO}$ were chosen sufficiently large to silence VLPO activity when F_{LC} and F_{DR} firing rates were high (as in waking).

The time constants (s) for the firing rate equations are given by

τ_{LC},	25;	τ_R,	1;	τ_{VLPO},	10;
τ_{DR},	25;	τ_{WR},	10;		

The ordering $\tau_R < \tau_{WR} = \tau_{VLPO} < \tau_{LC} = \tau_{DR}$ reflects the difference in activation rates between populations with autoexcitatory synapses and populations with autoinhibitory synapses. As described in RESULTS, this difference is necessary to obtain sufficiently long REM bout durations.

Inputs to the LC and DR populations include the term $\delta(t)$ that represents excitatory pulses of random amplitude (mean amplitude of 8 and SD of 0.1) that occur according to a Poisson process with an average rate of 0.003 Hz. The pulses instantaneously activate and decay exponentially with a time constant of 10 s.

For the neuronal populations LC, DR, R, and WR, the steady-state firing rate function has the form $F_{X\infty}(c) = X_{max}(0.5\{1 + \tanh[(c - \beta_X)/\alpha_X]\})$ with parameters as follows

LC_{max},	6.5 *Hz*;	α_{LC},	0.75;	β_{LC},	2;
DR_{max},	6.5 *Hz*;	α_{DR},	0.75;	β_{DR},	2;
R_{max},	5 *Hz*;	α_R,	0.25;	β_R,	−0.5;
WR_{max},	5 *Hz*;	α_{WR},	0.25;	β_{WR},	−0.2;
$VLPO_{max}$,	5 *Hz*;	α_{VLPO},	0.25;	$\beta_{VLPO}(h)$,	$-7h$;

Parameters describing maximal physiological firing rates of neuronal populations, X_{max} for $X = LC, DR, R, WR,$ and $VLPO$ were based on

experimental data (Aston-Jones and Bloom 1981; Datta and Siwek 2002; Hobson et al. 1975; Lydic et al. 1983; Steriade et al. 1990; Szymusiak et al. 1998; Trulson and Jacobs 1979; Wu et al. 1999, 2004). The α_X parameters control the slope of the sigmoid describing steady-state firing rates for each population; smaller parameters correspond to steeper slopes. Our choice of $\alpha_R = \alpha_{WR} = \alpha_{VLPO} < \alpha_{LC} = \alpha_{DR}$ reflects the autoinhibition in the LC and DR populations that dictates a slower activation rate (Hobson et al. 1975). The β_X parameters control the activation thresholds of each postsynaptic population. Therefore we chose the β_X in conjunction with the coupling parameters, $g_{i,X}$, to yield appropriate steady-state firing rates in the postsynaptic population in wake, NREM sleep, and REM sleep. The steady-state firing rate function for VLPO takes a similar form, but the threshold is modulated by the homeostatic sleep drive

$$F_{VLPO\infty}(c) = VLPO_{max}\,[0.5(1 + \tanh\{[c - \beta_{VLPO}(h)]/\alpha_{VLPO}\})] \tag{15}$$

For the neurotransmitters released by the LC, DR, VLPO, REM-active, and wake/REM-active populations, the normalized neurotransmitter concentrations $C_i(t)$ are determined by equations of the following form

$$C_i' = \frac{C_{i\infty}(F_X) - C_i}{\tau_i} \tag{16}$$

where $i = N$ for $X = LC$; $i = S$ for $X = DR$; $i = G$ for $X = VLPO$; $i = A(R)$ for $X = R$; and $i = A(WR)$ for $X = WR$. Total ACh concentration, C_A, released to postsynaptic populations is the sum of $C_{A(R)}$ and $C_{A(WR)}$.

The steady-state neurotransmitter release function, $C_{i\infty}(\cdot)$, is a saturating function of the form $C_{i\infty}(f) = \tanh(f/\gamma_i)$, and τ_i (s) is the time constant associated with neurotransmitter release at the population level. As noted previously, although current microdialysis techniques do not allow direct measurement of the rate constants of neurotransmitter release, τ_i for $i = N, S, A(R), A(WR)$, and G, we chose the time scale for these rate constants to be consistent with voltammetric data for the release and clearance of evoked dopamine (Garris and Wightman 1994). The slopes of the steady-state transmitter release functions (Hz) and time constant parameters (s) are

$$\gamma_N,\ 5;\quad \gamma_S,\ 5;\quad \gamma_{A(R)} = \gamma_{A(WR)},\ 3;\quad \gamma_G,\ 4;$$
$$\tau_N,\ 25;\quad \tau_S,\ 25;\quad \tau_{A(R)} = \tau_{A(WR)},\ 10;\quad \tau_G,\ 10;$$

The relative magnitudes of $\tau_{A(R)} = \tau_{A(WR)} = \tau_G < \tau_N = \tau_S$ reflect the faster action of ionotropic neurotransmitters ACh and GABA compared with the action of metabotropic NE and 5-HT (Destexhe et al. 1994). For each neurotransmitter, the steady-state function $C_{i\infty}(\cdot)$ is multiplicatively scaled by a random parameter $\sigma_i(t)$ (of normal distribution, unit mean and SD of 0.1) varying according to a Poisson process with an average rate of 10 Hz.

As described in METHODS, the homeostatic sleep drive, h, is governed by the following equation

$$h' = H[(F_{LC} + F_{DR}) - \theta_w]\frac{(1 - h)}{\tau_{hw}} - H[\theta_w - (F_{LC} + F_{DR})]\frac{h}{\tau_{hs}} \tag{17}$$

where $\theta_w = 3$ Hz and $H[z]$ is the Heaviside function defined as $H[z] = 0$ if $z < 0$ and $H[z] = 1$ if $z \geq 0$. The time constants for the increase of h during wake and its decrease during sleep states are $\tau_{hw} = 600$ s, and $\tau_{hs} = 320$ s, respectively.

For the simulations of microinjection of transmitter agonists and antagonists in the LC shown in Figs. 6–9, the governing equation for F_{LC} is

$$F_{LC}' = \frac{F_{LC\infty}[g_{A,LC}\,C_{A(LC)} - g_{N,LC}\,C_N - g_{G,LC}\,C_{G(LC)} + \delta(t)] - F_{LC}}{\tau_{LC}} \tag{18}$$

where the terms C_A and C_G in *Eq. 10* are replaced by $C_{A(LC)}$ and $C_{G(LC)}$, respectively, representing the effect of ACh and GABA in the LC. For the agonist microinjection simulations, $C_{A(LC)}$ and $C_{G(LC)}$ are given by the following expression

$$C_{i(LC)} = m_i(t)C_i + P_i \tag{19}$$

where $i = G$ and A. The term P_i represents the concentration of agonist and its decay is described by

$$P_i' = -\frac{P_i}{\tau_{Pi}} \tag{20}$$

with time constants set to $\tau_{Pi} = 10{,}000$ s. The factor $m_i(t)$ scales the level of endogenous neurotransmitter C_i in the LC according to the following rule

- $m_i(t) = 1$ if P_i levels are low (less than or equal to i_{min})
- $m_i(t) = 1 - (P_i - i_{min})/(i_{max} - i_{min})$ if P_i level are higher (greater than i_{min}).

Minimum and maximum values for GABA and ACh agonist concentrations are $G_{min} = 0.3$, $G_{max} = 2.5$, $A_{min} = 0.3$, and $A_{max} = 2$, respectively. For the antagonist microinjection simulations, total ACh and GABA concentration levels in the LC were scaled by the antagonist concentration, Q_i ($i = A$ and G). Thus in these simulations, $C_{A(LC)}$ and $C_{G(LC)}$ are given by the following expression

$$C_{i(LC)} = (1 - Q_i)C_i \tag{21}$$

where the decay of antagonist concentration is governed by

$$Q_i' = -\frac{Q_i}{\tau_{Qi}} \tag{22}$$

with time constants set to $\tau_{Qi} = 10{,}000$ s. Initial values for P_i and Q_i were zero in all simulations except in Figs. 6, 7, and 9, where microinjection of GABA agonist results were obtained with $P_G(0) = 2.0$ and GABA antagonist results with $Q_G(0) = 1.0$, and in Figs. 8 and 9, where ACh agonist microinjection was simulated by $P_A(0) = 0.8$ and ACh antagonist by $Q_A(0) = 0.55$. Values of these initial conditions were chosen such that agonist and antagonist effects were maintained over simulations of 4 h and produced distinguishable changes in sleep-wake microarchitecture. Larger or smaller values of initial conditions resulted in the same qualitative changes in sleep-wake patterning but with differences in the magnitude of the effects.

ACKNOWLEDGMENTS

We thank H. Baghdoyan, D. Forger, and R. Lydic for helpful discussions of this work.

GRANTS

This work was supported by Air Force Office of Scientific Research FA9550-08-1-0111.

REFERENCES

Arnsten AF, Goldman-Rakic PS. Selective prefrontal cortical projections to the region of the locus coeruleus and raphe nuclei in the rhesus monkey. *Brain Res* 306: 9–18, 1984.

Aston-Jones G, Bloom FE. Activity of norepinephrine-containing locus coeruleus neurons in behaving rats anticipates fluctuations in the sleep-waking cycle. *J Neurosci* 1: 876–886, 1981.

Baghdoyan HA. Location and quantification of muscarinic receptor subtypes in rat pons: implications for REM sleep generation. *Am J Physiol* 273: R896–R904, 1997.

Basheer R, Porkka-Heiskanen T, Stenberg D, McCarley RW. Adenosine and behavioral state control: adenosine increases c-Fos protein and AP1 binding in basal forebrain of rats. *Brain Res Mol Brain Res* 73: 1–10, 1999.

Basheer R, Strecker RE, Thakkar MM, McCarley RW. Adenosine and sleep-wake regulation. *Prog Neurobiol* 73: 379–396, 2004.

Benington JH, Heller HC. Does the function of REM sleep concern non-REM sleep or waking? *Prog Neurobiol* 44: 433–449, 1994.

Blanco-Centurion C, Gerashchenko D, Shiromani PJ. Effects of saporin-induced lesions of three arousal populations on daily levels of sleep and wake. *J Neurosci* 27: 14041–14048, 2007.

Borbely AA. A two process model of sleep regulation. *Hum Neurobiol* 1: 195–204, 1982.

Borbely AA, Achermann P. Sleep homeostasis and models of sleep regulation. *J Biol Rhythms* 14: 557–568, 1999.

Brown RE, McKenna JT, Winston S, Basheer R, Yanagawa Y, Thakkar MM, McCarley RW. Characterization of GABAergic neurons in rapid-eye-movement sleep controlling regions of the brainstem reticular formation in GAD67-green fluorescent protein knock-in mice. *Eur J Neurosci* 27: 352–363, 2008.

Brown RE, Winston S, Basheer R, Thakkar MM, McCarley RW. Electrophysiological characterization of neurons in the dorsolateral pontine rapid-eye-movement sleep induction zone of the rat: intrinsic membrane properties and responses to carbachol and orexins. *Neuroscience* 143: 739–755, 2006.

Carskadon MA, Dement WC. Normal human sleep: an overview. In: *Principles and Practice of Sleep Medicine*, edited by Kryger M, Roth T, Dement WC. New York: Saunders, 2000, p. 15–25.

Chamberlin NL, Arrigoni E, Chou TC, Scammell TE, Greene RW, Saper CB. Effects of adenosine on gabaergic synaptic inputs to identified ventrolateral preoptic neurons. *Neuroscience* 119: 913–918, 2003.

Datta S, Maclean RR. Neurobiological mechanisms for the regulation of mammalian sleep-wake behavior: reinterpretation of historical evidence and inclusion of contemporary cellular and molecular evidence. *Neurosci Biobehav Rev* 31: 775–824, 2007.

Datta S, Siwek DF. Single cell activity patterns of pedunculopontine tegmentum neurons across the sleep-wake cycle in the freely moving rats. *J Neurosci Res* 70: 611–621, 2002.

Dayan P, Abbott LF. *Theoretical Neuroscience: Computational and Mathematical Modeling of Neural Systems.* Cambridge, MA: MIT Press, 2001.

Deco G, Jirsa VK, Robinson PA, Breakspear M, Friston K. The dynamic brain: from spiking neurons to neural masses and cortical fields. *PLoS Comput Biol* 4: e1000092, 2008.

Destexhe A, Contreras D, Sejnowski TJ, Steriade M. Modeling the control of reticular thalamic oscillations by neuromodulators. *Neuroreport* 5: 2217–2220, 1994.

Diniz Behn CG, Brown EN, Scammell TE, Kopell NJ. A mathematical model of network dynamics governing mouse sleep-wake behavior. *J Neurophysiol* 97: 3828–3840, 2007.

Dzirasa K, Ribeiro S, Costa R, Santos LM, Lin SC, Grosmark A, Sotnikova TD, Gainetdinov RR, Caron MG, Nicolelis MA. Dopaminergic control of sleep-wake states. *J Neurosci* 26: 10577–10589, 2006.

Egan TM, North RA. Acetylcholine acts on m2-muscarinic receptors to excite rat locus coeruleus neurones. *Br J Pharmacol* 85: 733–735, 1985.

Egan TM, North RA. Acetylcholine hyperpolarizes central neurones by acting on an M2 muscarinic receptor. *Nature* 319: 405–407, 1986.

Ennis M, Shipley MT. Tonic activation of locus coeruleus neurons by systemic or intracoerulear microinjection of an irreversible acetylcholinesterase inhibitor: increased discharge rate and induction of C-fos. *Exp Neurol* 118: 164–177, 1992.

Ermentrout GB. Neural networks as spatio-temporal pattern-forming systems. *Rep Prog Phys* 61: 353–430, 1998.

Gallopin T, Luppi PH, Cauli B, Urade Y, Rossier J, Hayaishi O, Lambolez B, Fort P. The endogenous somnogen adenosine excites a subset of sleep-promoting neurons via A2A receptors in the ventrolateral preoptic nucleus. *Neuroscience* 134: 1377–1390, 2005.

Garris PA, Wightman RM. Different kinetics govern dopaminergic transmission in the amygdala, prefrontal cortex, and striatum: an in vivo voltammetric study. *J Neurosci* 14: 442–450, 1994.

Gerber U, Stevens DR, McCarley RW, Greene RW. Muscarinic agonists activate an inwardly rectifying potassium conductance in medial pontine reticular formation neurons of the rat in vitro. *J Neurosci* 11: 3861–3867, 1991.

Gervasoni D, Darracq L, Fort P, Souliere F, Chouvet G, Luppi PH. Electrophysiological evidence that noradrenergic neurons of the rat locus coeruleus are tonically inhibited by GABA during sleep. *Eur J Neurosci* 10: 964–970, 1998.

Gervasoni D, Peyron C, Rampon C, Barbagli B, Chouvet G, Urbain N, Fort P, Luppi PH. Role and origin of the GABAergic innervation of dorsal raphe serotonergic neurons. *J Neurosci* 20: 4217–4225, 2000.

Hobson JA, McCarley RW, Wyzinski PW. Sleep cycle oscillation: reciprocal discharge by two brainstem neuronal groups. *Science* 189: 55–58, 1975.

Huang ZL, Urade Y, Hayaishi O. Prostaglandins and adenosine in the regulation of sleep and wakefulness. *Curr Opin Pharmacol* 7: 33–38, 2007.

Iijima K, Ohtomo K. Immunocytochemical study using a GABA antiserum for the demonstration of inhibitory neurons in the rat locus ceruleus. *Am J Anat* 181: 43–52, 1988.

Jodo E, Chiang C, Aston-Jones G. Potent excitatory influence of prefrontal cortex activity on noradrenergic locus coeruleus neurons. *Neuroscience* 83: 63–79, 1998.

Kalinchuk AV, McCarley RW, Stenberg D, Porkka-Heiskanen T, Basheer R. The role of cholinergic basal forebrain neurons in adenosine-mediated homeostatic control of sleep: lessons from 192 IgG-saporin lesions. *Neuroscience* 157: 238–253, 2008.

Kalsner S. Heteroreceptors, autoreceptors and other terminal sites. In: *Presynaptic Receptors and the Question of Autoregulation of Neurotransmitter Release*, edited by Kalsner S, Westfall TC. New York: New York Academy of Sciences, 1990, p. 1–6.

Kawahara Y, Kawahara H, Westerink BH. Tonic regulation of the activity of noradrenergic neurons in the locus coeruleus of the conscious rat studied by dual-probe microdialysis. *Brain Res* 823: 42–48, 1999.

Liu ZW, Gao XB. Adenosine inhibits activity of hypocretin/orexin neurons by the A1 receptor in the lateral hypothalamus: a possible sleep-promoting effect. *J Neurophysiol* 97: 837–848, 2007.

Lo CC, Chou T, Penzel T, Scammell TE, Strecker RE, Stanley HE, Ivanov P. Common scale-invariant patterns of sleep-wake transitions across mammalian species. *Proc Natl Acad Sci USA* 101: 17545–17548, 2004.

Lu J, Devor M, Saper C. A pontine tegmental flip-flop switch for regulation of REM sleep. *Soc Neurosci Abst* 895.896, 2004.

Lu J, Sherman D, Devor M, Saper CB. A putative flip-flop switch for control of REM sleep. *Nature* 441: 589–594, 2006.

Luppi PH, Gervasoni D, Verret L, Goutagny R, Peyron C, Salvert D, Leger L, Fort P. Paradoxical (REM) sleep genesis: the switch from an aminergic-cholinergic to a GABAergic-glutamatergic hypothesis. *J Physiol Paris* 100: 271–283, 2006.

Lydic R, Baghdoyan HA. Pedunculopontine stimulation alters respiration and increases ACh release in the pontine reticular formation. *Am J Physiol* 264: R544–R554, 1993.

Lydic R, Baghdoyan HA. Sleep, anesthesiology, and the neurobiology of arousal state control. *Anesthesiology* 103: 1268–1295, 2005.

Lydic R, Baghdoyan HA. Acetylcholine modulates sleep and wakefulness: a synaptic perspective. In: *Neurochemistry of Sleep and Wakefulness*, edited by Monti JM, Pandi-Perumal SR, Sinton CM. Cambridge, MA: Cambridge University Press, 2008, p. 109–143.

Lydic R, McCarley RW, Hobson JA. The time-course of dorsal raphe discharge, PGO waves, and muscle tone averaged across multiple sleep cycles. *Brain Res* 274: 365–370, 1983.

Mallick BN, Kaur S, Saxena RN. Interactions between cholinergic and GABAergic neurotransmitters in and around the locus coeruleus for the induction and maintenance of rapid eye movement sleep in rats. *Neuroscience* 104: 467–485, 2001.

Massaquoi SG, McCarley RW. Extension of the limit cycle reciprocal interaction model of REM cycle control. An integrated sleep control model. *J Sleep Res* 1: 138–143, 1992.

Masserano JM, King C. Effects on sleep of acetylcholine perfusion of the locus coeruleus of cats. *Neuropharmacology* 21: 1163–1167, 1982.

McCarley RW, Hobson JA. Neuronal excitability modulation over the sleep cycle: a structural and mathematical model. *Science* 189: 58–60, 1975.

Morairty S, Rainnie D, McCarley R, Greene R. Disinhibition of ventrolateral preoptic area sleep-active neurons by adenosine: a new mechanism for sleep promotion. *Neuroscience* 123: 451–457, 2004.

Nakamura T, Uramura K, Nambu T, Yada T, Goto K, Yanagisawa M, Sakurai T. Orexin-induced hyperlocomotion and stereotypy are mediated by the dopaminergic system. *Brain Res* 873: 181–187, 2000.

Nitz D, Siegel J. GABA release in the dorsal raphe nucleus: role in the control of REM sleep. *Am J Physiol* 273: R451–R455, 1997.

Osmanovic SS, Shefner SA. gamma-Aminobutyric acid responses in rat locus coeruleus neurones in vitro: a current-clamp and voltage-clamp study. *J Physiol* 421: 151–170, 1990.

Peyron C, Tighe DK, van den Pol AN, de Lecea L, Heller HC, Sutcliffe JG, Kilduff TS. Neurons containing hypocretin (orexin) project to multiple neuronal systems. *J Neurosci* 18: 9996–10015, 1998.

Phillips AJ, Robinson PA. A quantitative model of sleep-wake dynamics based on the physiology of the brainstem ascending arousal system. *J Biol Rhythms* 22: 167–179, 2007.

Phillips AJ, Robinson PA. Sleep deprivation in a quantitative physiologically based model of the ascending arousal system. *J Theor Biol* 255: 413–423, 2008.

Porkka-Heiskanen T, Strecker RE, McCarley RW. Brain site-specificity of extracellular adenosine concentration changes during sleep deprivation and spontaneous sleep: an in vivo microdialysis study. *Neuroscience* 99: 507–517, 2000.

Porkka-Heiskanen T, Strecker RE, Thakkar M, Bjorkum AA, Greene RW, McCarley RW. Adenosine: a mediator of the sleep-inducing effects of prolonged wakefulness. *Science* 276: 1265–1268, 1997.

Portas CM, Thakkar M, Rainnie DG, Greene RW, McCarley RW. Role of adenosine in behavioral state modulation: a microdialysis study in the freely moving cat. *Neuroscience* 79: 225–235, 1997.

Rainnie DG, Grunze HC, McCarley RW, Greene RW. Adenosine inhibition of mesopontine cholinergic neurons: implications for EEG arousal. *Science* 263: 689–692, 1994.

Rempe MJ, Best J, Terman D. A mathematical model of the sleep/wake cycle. *J Math Biol* doi:10.1007/s00285-009-0276-5.

Rye D, Jankovic J. Emerging views of dopamine in modulating sleep/wake state from an unlikely source: PD. *Neurology* 58: 341–346, 2002.

Saper CB, Chou TC, Scammell TE. The sleep switch: hypothalamic control of sleep and wakefulness. *Trends Neurosci* 24: 726–731, 2001.

Saper CB, Scammell TE, Lu J. Hypothalamic regulation of sleep and circadian rhythms. *Nature* 437: 1257–1263, 2005.

Sapin E, Lapray D, Berod A, Goutagny R, Leger L, Ravassard P, Clement O, Hanriot L, Fort P, Luppi PH. Localization of the brainstem GABAergic neurons controlling paradoxical (REM) sleep. *PLoS One* 4: e4272, 2009.

Starke K, Gothert M, Kilbinger H. Modulation of neurotransmitter release by presynaptic autoreceptors. *Physiol Rev* 69: 864–989, 1989.

Steriade M, Datta S, Pare D, Oakson G, Curro Dossi RC. Neuronal activities in brain-stem cholinergic nuclei related to tonic activation processes in thalamocortical systems. *J Neurosci* 10: 2541–2559, 1990.

Steyn-Ross DA, Steyn-Ross ML, Sleigh JW, Wilson MT, Gillies IP, Wright JJ. The sleep cycle modelled as a cortical phase transition. *J Biol Phys* 31: 547–569, 2005.

Szymusiak R, Alam N, Steininger TL, McGinty D. Sleep-waking discharge patterns of ventrolateral preoptic/anterior hypothalamic neurons in rats. *Brain Res* 803: 178–188, 1998.

Tamakawa Y, Karashima A, Koyama Y, Katayama N, Nakao M. A quartet neural system model orchestrating sleep and wakefulness mechanisms. *J Neurophysiol* 95: 2055–2069, 2006.

Thakkar MM, Strecker RE, McCarley RW. Behavioral state control through differential serotonergic inhibition in the mesopontine cholinergic nuclei: a simultaneous unit recording and microdialysis study. *J Neurosci* 18: 5490–5497, 1998.

Thakkar MM, Winston S, McCarley RW. A1 receptor and adenosinergic homeostatic regulation of sleep-wakefulness: effects of antisense to the A1 receptor in the cholinergic basal forebrain. *J Neurosci* 23: 4278–4287, 2003.

Thannickal TC, Moore RY, Nienhuis R, Ramanathan L, Gulyani S, Aldrich M, Cornford M, Siegel JM. Reduced number of hypocretin neurons in human narcolepsy. *Neuron* 27: 469–474, 2000.

Trulson ME, Jacobs BL. Raphe unit activity in freely moving cats: correlation with level of behavioral arousal. *Brain Res* 163: 135–150, 1979.

Van Dort CJ, Baghdoyan HA, Lydic R. Adenosine A(1) and A(2A) receptors in mouse prefrontal cortex modulate acetylcholine release and behavioral arousal. *J Neurosci* 29: 871–881, 2009.

Vanni-Mercier G, Sakai K, Lin JS, Jouvet M. Mapping of cholinoceptive brainstem structures responsible for the generation of paradoxical sleep in the cat. *Arch Ital Biol* 127: 133–164, 1989.

Watson CJ, Venton BJ, Kennedy RT. In vivo measurements of neurotransmitters by microdialysis sampling. *Anal Chem* 78: 1391–1399, 2006.

Weitzman ED, Czeisler CA, Zimmerman JC, Ronda J. The timing of REM sleep and its relation to spontaneous awakenings during temporal isolation in man. *Sleep Res* 9: 280, 1980.

Wilson HR, Cowan JD. Excitatory and inhibitory interactions in localized populations of model neurons. *Biophys J* 12: 1–24, 1972.

Wilson MT, Steyn-Ross DA, Sleigh JW, Steyn-Ross ML, Wilcocks LC, Gillies IP. The K-complex and slow oscillation in terms of a mean-field cortical model. *J Comput Neurosci* 21: 243–257, 2006.

Wilson MT, Steyn-Ross ML, Steyn-Ross DA, Sleigh JW. Predictions and simulations of cortical dynamics during natural sleep using a continuum approach. *Phys Rev E Stat Nonlin Soft Matter Phys* 72: 051910, 2005.

Wu MF, Gulyani SA, Yau E, Mignot E, Phan B, Siegel JM. Locus coeruleus neurons: cessation of activity during cataplexy. *Neuroscience* 91: 1389–1399, 1999.

Wu MF, John J, Boehmer LN, Yau D, Nguyen GB, Siegel JM. Activity of dorsal raphe cells across the sleep-waking cycle and during cataplexy in narcoleptic dogs. *J Physiol* 554: 202–215, 2004.